Title

PREFERENTIAL POLAR ALPHA-PARTICLE EMISSION IN ORIENTED CALIFORNIUM AND EINSTEINIUM

Author

Navarro, Quirino Oli.

Publication Date

1962-07-12

Thesis/dissertation

UCRL 10362

University of California

Ernest O. Lawrence Radiation Laboratory

PREFERENTIAL POLAR ALPHA-PARTICLE EMISSION IN ORIENTED CALIFORNIUM AND EINSTEINIUM

Berkeley, California

DISCLAIMER

Research and Development

UCRL-10362
UC-4 Chemistry
TID-4500 (17th Ed.)

UNIVERSITY OF CALIFORNIA

Lawrence Radiation Laboratory
Berkeley, California

Contract No. 7405-eng-48

PREFERENTIAL POLAR ALPHA-PARTICLE EMISSION IN ORIENTED CALIFORNIUM AND EINSTEINIUM

Quirino Oli Navarro

(Ph.D. Thesis)

July 12, 1962

Printed in USA. Price $2.00. Available from the
Office of Technical Services
U. S. Department of Commerce
Washington 25, D.C.

PREFERENTIAL POLAR ALPHA-PARTICLE EMISSION IN ORIENTED CALIFORNIUM AND EINSTEINIUM

Contents

PREFERENTIAL POLAR ALPHA-PARTICLE EMISSION IN ORIENTED CALIFORNIUM AND EINSTEINIUM

Quirino Oli Navarro

Lawrence Radiation Laboratory
University of California
Berkeley, California

July 12, 1962

ABSTRACT

Nuclear alignment experiments were performed on E^{253} and Cf^{249}, incorporated as the tripositive ions, in single crystals $Nd(C_2H_5SO_4)_3 \cdot 9H_2O$. The actinides and lanthanides were shown to be isomorphous in this salt. The low temperatures needed were attained by adiabatic demagnetization of the samples. Alpha particles emitted from the samples and detected with germanium surface-barrier detectors were found to be highly anisotropic; in the case of einsteinium the nuclear orientation was saturated at a relatively high temperature. The alpha particles from these nuclei were shown to be preferentially emitted from the "tips," thus providing two independent confirmations of the prediction of Hill and Wheeler. The S- and D-waves in the "favored" transitions in these isotopes were found to be in phase. The L = 2, 4 waves in einsteinium were interpreted as being out of phase; the L = 3,5 components in californium could not be determined with certainty, although an out-of-phase relationship was indicated.

By use of the theory of Elliott and Stevens, the electronic ground state resulting from the crystal-field splitting of the ground level of tripositive einsteinium in $Nd(C_2H_5SO_4)_3 \cdot 9H_2O$ was calculated. It was found that the theory, developed for the lanthanides, can be applied to the actinides as well. Values of $\langle r^{-3} \rangle$ for the 5f electrons were estimated; these values and the above theory were used in deriving values of the nuclear moments. From assumed nuclear spins I = 7/2 and I = 9/2 for E^{253} and Cf^{249}, respectively, nuclear moments of $|\mu_{253}|$ = 4.9 n.m. and $|\mu_{249}|$ = 1.3 n.m. were derived. Errors of about 20% ,

of which one-half comes from uncertainties in the theory, should be attached to these values.

The gamma rays of Cm^{245}, following the alpha decay of Cf^{249}, were found to be anisotropic. Appreciable attenuation of the gamma-rays was found, indicating some reorientation of the nuclear spin of the daughter nucleus.

Nuclear-alignment experiments were also performed on Dy^{155} and Dy^{157}. The angular distributions of the gamma rays following the decays of both isotopes were found to be anisotropic. Spin 5/2-was assigned to the states at 227 keV in Tb^{155} and at 327 keV in Tb^{157}. The nuclear moments $|\mu_{155}| = 0.21 \pm 0.05$ n.m. and $|\mu_{157}| = 0.32 \pm 0.02$ n.m. were derived, based on $I = 3/2$ for both isotopes as well as pure $L = 1$ beta decay to the $5/2$ - states.

The practicality of germanium surface-barrier detectors was again demonstrated. It was found that these are suitable for use at low temperatures for detecting alpha and beta particles. Experiments indicated that under the conditions demanded in this line of investigation, these detectors are superior to other means of detection of charged particles.

I. INTRODUCTION

Various methods have been devised and utilized in the study of nuclear properties of the elements. One method that has been used successfully in the study of the lanthanide and actinide elements is nuclear orientation. The technique involves observation of quanta emitted from nuclei oriented at low temperatures. The method requires an assembly of radioactive nuclei, some means for detection and measurement of the quanta, and some method for obtaining the necessary low temperature.

There is no particular problem in the detection of sufficiently energetic gamma rays, because these can penetrate the cryostat walls and scintillation detectors can be used. However, alpha particles cannot penetrate the walls of the cryostat and the detectors themselves must be within the cryostat. Thus, particle detectors must meet certain requirements of size, ability to work at low pressures and temperatures near $1^{\circ}K$, and very high detection efficiency. The usual methods of detection are either completely useless or very inefficient, but germanium surface-barrier detectors have met these requirements for the most part. The requisite low temperatures can easily be attained by adiabatic demagnetization of a salt crystal in which the activity is incorporated. The direction of orientation can be referred either to a crystalline axis of the host crystal or to the direction of an applied external magnetic field.

The nuclear properties can usually be deduced from the angular distribution of the emitted gamma rays in cases where no detectable charged particles are emitted (e.g., electron capture, isomeric transition). If the nucleus of interest emits charged particles (α, β, or fission fragments), the angular distribution of these particles and (or) the gamma rays following the decay may be measured. From the measured angular distribution and its temperature dependence, one can determine indirectly the nuclear moment, the angular momenta removed during radioactive decay, angular momenta or "spins" of excited states, and mixing ratios of different multipoles. Thus, in charged-particle emission,

the direction of preferential emission and the partial-wave intensities may be determined. As with any experiment, comparison of experimental values with theory is extremely important. The nuclear-alignment data may be used to confirm values obtained by other methods. These data may also be used to establish unambiguously quantities which cannot be obtained by other methods.

In this thesis are described experiments in which only gamma rays are observed (Dy^{155} and Dy^{157}), only alpha particles are measured (E^{253}), and in which alpha particles and the ensuing gamma rays are detected (Cf^{249}). A brief description of the preparation of the germanium surface-barrier counters that were used is also included.

II. APPARATUS

A. Magnet

The magnet was powered by a 100 kVA motor-generator set provided with variable current control for the magnet windings. It was capable of producing fields up to 18 kG over a 3-in. pole gap.

B. Mutual-Inductance System

The temperatures attained after demagnetization were determined by magnetic-susceptibility measurements on the sample. The detecting coil was 750 turns of B.S. No. 40 Formvar-insulated copper wire on the primary and on each of two secondaries. An ac bridge was used for balancing the mutual inductance of the secondary coils with a known inductance. More complete descriptions of the magnet and the mutual-inductance bridge systems are found in earlier papers.[1-3]

C. Cryostat

The cryostat assembly is shown in Fig. 1.

All demagnetization cryostats must have a thermal reservoir and a chamber wherein the sample can be thermally isolated from the reservoir at will. The bath in these experiments was liquid helium contained in a dewar A surrounded by another dewar B containing liquid nitrogen. Both dewars were made from pyrex tubing. The inside walls were silvered except for two 1/2 - in. wide vertical strips at 180 deg for viewing the liquid-helium level. A vacuum stopcock C was provided on the helium dewar for repumping between experiments, because helium gas diffuses through borosilicate glasses.

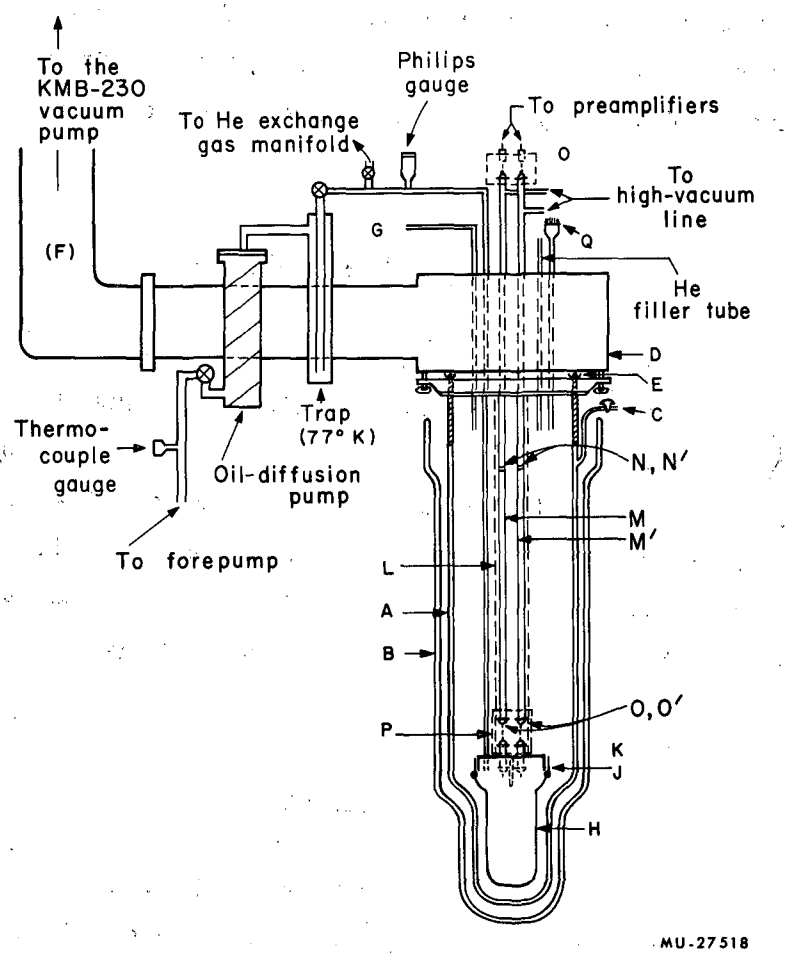

Fig. 1. Adiabatic demagnetization apparatus.

The helium dewar was bolted to the steel head D with a rubber o-ring and pyrex pipe flange E, providing a vacuum-tight seal. The bath temperature could be lowered to near 1°K by pumping off the vapor from the reservoir of liquid helium. A Kinney KMB-230 vacuum pump F was used. The vapor pressure of the liquid helium was measured by means of two manometers connected to the bath through a tube G: a mercury manometer was used for pressures above about the λ point of liquid helium; below this point, a dibutylphthalate manometer provided a more accurate pressure indication. The temperature of the bath was determined from the pressure reading and the known vapor-pressure—temperature relationship for liquid helium-4 (see IV-C).

The sample chamber H is made from a commercially available copper-pyrex housekeeper seal J. It was soft-soldered to the cap K which is part of the mechanical support L. A 1/8-in.-diam stainless steel tube passing through the cap was used to evacuate the sample chamber. This tube was connected to a valve assembly which permitted evacuation of the chamber or introduction of helium exchange gas to allow thermal contact of the sample with the bath. The pressure inside the chamber was determined by means of a Philips electron gauge.

The cap K also provided means for supporting the counter and sample assemblies, details of which are shown in Fig. 2 and discussed in sections D and E. The sample assembly was held in place by a glass rod sealed to a tungsten rod which was hard-soldered to the cap. A nut soldered to the underside of the cap held the counter cage.

The tubes M and M' were 1/2-in.-diam tubes which acted as shields for the signal leads from the alpha-particle detectors. These tubes were continuously evacuated by oil-diffusion vacuum pumps backed by mechanical pumps because otherwise moisture tended to collect inside the shields when the apparatus was not in use, causing electrical shorts. The signal leads inside these shields were of manganin wire held concentric with the tubes by ceramic spacers N and N'. The wires terminated in Kovar seals O and O' soldered to the ends of the shielding tubes.

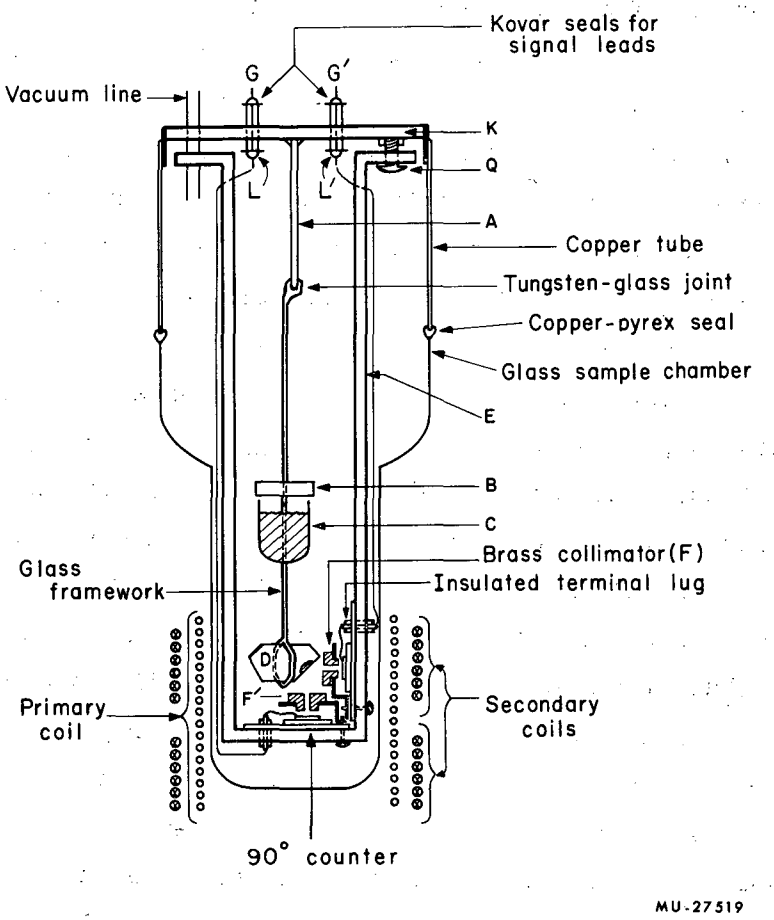

Fig. 2. Sample and counter cage assemblies.

Connections to the preamplifiers were made with properly shielded wires terminating in standard BNC connectors. Joints between the shielded leads and the Kovar seals on the cap were shielded during the experiments by wrapping a grounded piece of aluminum foil P around the areas of the joints.

The inductance coils were connected to the bridge through Kovar seal Q.

D. Sample Assembly

Figure 2 shows the sample chamber, the sample assembly, and the counter cage.

A length of tungsten rod A hard-soldered to the cap K held the glass framework. The sample framework held the pill of manganous ammonium sulfate B , the small glass cap C containing a few cubic centimeters of chrome-alum-glycerol slurry, and the sample D . The pill of manganous ammonium sulfate and the slurry shielded the sample, after adiabatic demagnetization, from black-body radiation originating from parts of the apparatus that were not at the temperature of the bath, as well as from heat leaks arising from residual gas or conduction down the support.

E. Counter Cage Assembly

The counter cage E was made from a thin brass tube. Most of the metal was cut away leaving only two narrow vertical strips and cylindrical sections at the ends. A disc was soldered to the lower end to hold the 90-deg counter; one of the vertical strips held the 0-deg counter. Two collimators (F, F') were mounted on brass supports held in front of the counters by the screws that secured the counters to the cage. The collimators were made from brass tubes with a 0.064-in. bore. The signal leads from the counters passed through Kovar seals

(G, G' and L, L') and were brought to the amplifying system through the shielding tubes M, M' of Fig. 1. The counter cage was held to the cap by the screw Q.

F. Alpha-Counter Amplifying Systems

The pulses from the detectors were fed to low-noise charge-sensitive UCLRL Model-5V1012 preamplifiers, the outputs of which were applied to respective Model-V linear amplifers (UCLRL-5V1034). The amplified signals were fed directly to pulse-height analyzers. In cases where separation of the different alpha groups was desired, the amplified signals could be fed first to biased amplifiers (UCLRL Model-5V1002) before pulse-height analysis. In these experiments, the nature of the source precluded any possibility of distinguishing the different alpha groups, so that biased amplifiers were not used. A complete circuit description of the biased amplifier and preamplifier is given by Goulding and Hansen.[4]

G. Gamma-Counting Equipment

For the detection of gamma rays, 3-by 3-in. cylindrical NaI(Tl) scintillation crystals were used. These were optically joined to photo-multiplier tubes. The output pulses were fed to cathode followers and amplified by DD2 amplifiers. The output of these amplifiers were than fed to pulse-height analyzers.

H. Pulse-Height Analyzers

In the work on dysprosium, the signals from both DD2 linear amplifiers were sent to 100-channel differential pulse-height analyzers.

With the acquisition of a Technical Measurements Corporation Model-213 pulse-height analyzer, four separate input sources could be handled simultaneously. This model incorporates an automatic print-out unit, so that once started, the analyzer would count for the intervals

desired, print-out the information, and automatically recycle itself. Blocking time can also be corrected automatically. With this unit, it was possible to continuously count the signals from the alpha-and gamma-ray counters simultaneously. The detecting, amplifying, and analyzing systems are shown in block diagram in Fig. 3.

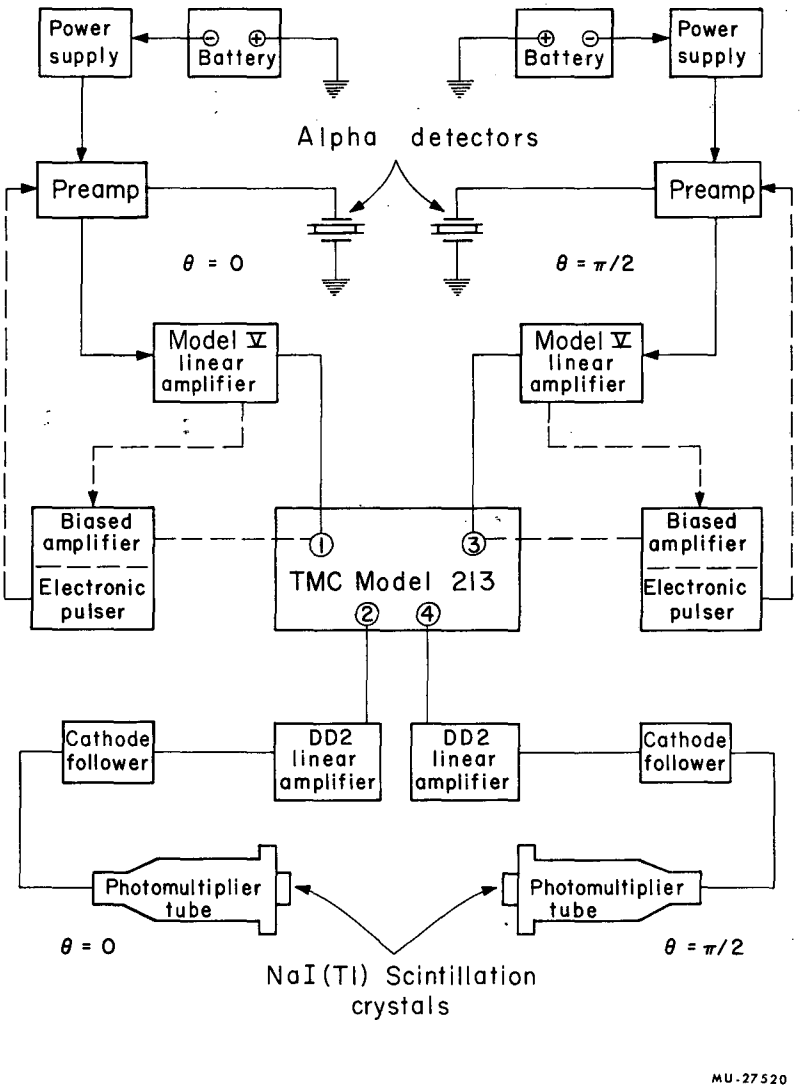

Fig. 3. Alpha and gamma counting systems.

III. ALPHA-PARTICLE DETECTORS

A. Preparation

The alpha-particle counters were the surface-barrier type.[5] Three different techniques were employed in their preparation.

1. Method I

A 50-mil-thick wafer was cut with a diamond wheel from a carefully oriented single crystal of 30 ohm-cm n-type germanium along the [111] plane. It was cut into 8-by-8 mm plates and hand-lapped with a 400-mesh silicon carbide slurry in water. It was rinsed with water and dipped in an etching solution of HNO_3-HF acid mixture for several minutes. Then it was washed successively with water, methanol, and ethylene trichloride. A stream of dry nitrogen gas was used to dry the plates prior to mounting them in the evaporator. Gold evaporated from a tungsten filament was deposited on one side of each plate to a thickness of from several hundred to a few thousand angstroms. A molybdenum strip, provided with holes for an insulated terminal lug and a screw, was similarly coated with gold. A piece of gold foil was sandwiched between the coated sides of the plate and the molybdenum strip. It was heated under compression in a furnace until the gold had alloyed with the germanium and the plate "sweated" onto the strip. Upon cooling, it was etched, washed, and dried as before, and the germanium portion was coated with gold. A circular mask of picein wax was put on the front of the germanium and the exposed surface was etched again. It was then freed of acid and dried with dry nitrogen gas. A short piece of 5-mil gold wire was pressure-bonded to the gold-coated surface on the plate. An insulated terminal lug was pressed in place and the other end of the gold wire was spot-welded to the lug. A counter made by this method is shown in Fig. 4a.

2. Method II

Plates 1 cm square and 1 mm thick were cut and hand-lapped as in Method I. These were then etched with CP-4 etch* until the reaction had

---

* The CP-4 etch is five parts by volume concentrated HNO_3, three parts by volume 48% HF, and three parts by volume glacial acetic acid.

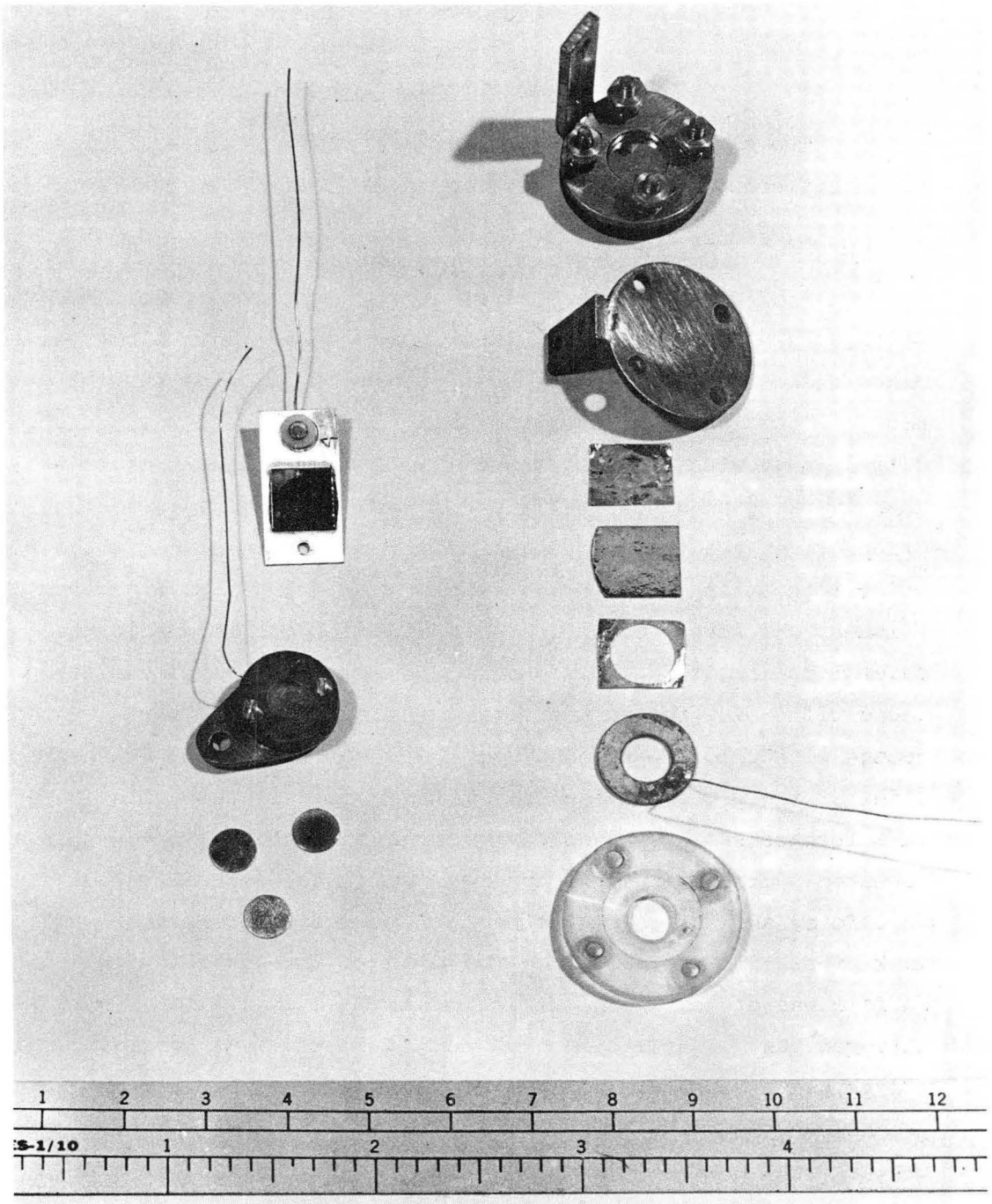

ZN-3205

Fig. 4. (a) Germanium surface-barrier counter used in alpha experiments, Method I; (b) germanium counter components and assembled counter, Method II; (c) alloyed germanium discs and assembled counter, Method III.

subsided. The plates were then washed with deionized water and allowed to dry in air. The surfaces of each plate were cleaned by ion-bombardment just prior to gold deposition. A layer of gold several thousand angstroms thick was deposited on the surfaces of each plate. The front and back surfaces were masked with picein wax, and the exposed edges were etched with CP-4 etch. The plates were then washed in a continuous stream of deionized water for several minutes and then laid on a piece of filter paper and allowed to dry. When the plates had dried, they were mounted in crystal holders.

Each crystal holder consisted of:

(a) a front plate. This was made of 1/16-in.-thick hard rubber, lucite, or laminated canvas disc about 3/4 in. in diameter. A 3/16-in.-diam hole was drilled at the center of each disc. A shallow groove was also cut along the periphery of the hole to hold the front-face electrode. A small hole was provided for the signal lead from the front-face electrode.

(b) a back plate. This was made of 1/16-in.-thick brass bent to form a bracket for mounting to the crystal cage. Four spring-loaded screws secure the front plate to the backing plate.

(c) a front-face electrode. A short piece of copper wire was soldered to a thin brass ring. The brass ring fitted into the groove of the front plate and the copper wire was passed through the hole provided for the purpose.

(d) front and back face gaskets. These were made of square sections of 5-mil gold or indium foil. The front-face gasket has its center cut out to allow passage of particles.

The detector was sandwiched between the gaskets and then secured in position by four spring-loaded screws, between the back and front plate. The back plate served as a ground connection. All detectors made by this method were unsuccessful. Figure 4b shows the parts of the detector and the assembled counter.

3. Method III

Discs about 0.25 in. in diameter were cut supersonically from a 50-mil-thick wafer. After hand-lapping and etching, gold was evaporated onto the cleaned and dried surfaces, then heated in a furnace to alloy the gold with the germanium. These were then mounted in crystal holders similar to those of Method II. No gaskets and brass ring were used. Electrical connection to the front surface was made by pressing a short piece of 5-mil gold wire between the front plate and the detector. Figure 4c shows some alloyed discs and the assembled counter. As in Method II, no successful counters were obtained.

B. Operating Characteristics

1. Effect of Stray Capacitance

If the rise time of the pulse is appreciably shorter than the time constant $R_T(C_c + C_p)$, the size of the pulse, v , which occurs across the counter is given by[6]

$$v = \frac{eW\eta}{(C_c + C_p)\epsilon} ,$$

where C_c is the capacitance of the counter, C_p is the stray capacitance to ground in parallel with the counter, W is the total energy lost by ionizing particle within the region of appreciable electric field, e is the magnitude of the charge on the electron, ϵ is the average amount of energy required to create a free electron-hole pair, η is the apparent efficiency of charge collection, and $1/R_T = 1/R_c + 1/R_p$, where R_p is the total resistance to ground in parallel with the counter. In these detectors the rise time is very much shorter than the time constant, so that the above equation is obeyed. Note that it is important to have as little stray capacitance as possible. The length of the leads and the method of shielding greatly affect the amount of stray capacitance. In the setup used in the alpha experiments, the minimum

total capacitance of each counting system, before the preamplification stage, attained at 1.1°K with no bias voltage was 70 pF. The effective resistance was several hundred megohms. The effective resistance varies from experiment to experiment, depending on the amount of leakage to ground. The resistances of the counters used were approximately 30 and 50 ohms at room temperature and increased to several hundred megohms at helium temperatures.

2. Effect of Bias Voltage

The pulse height obtained increased with increasing negative voltage on the front of the counter. This is shown in Fig. 5. The signal-to-noise ratio improved with increased negative voltage until the breakdown voltage was approached. The breakdown voltage was usually around -30 V at 77°K, and somewhat lower at 1.1°K. The effect of bias voltage on the resolution is shown in Fig. 6. The figure shows the beta spectrum from a Hg^{203} source deposited on aluminized mylar.

3. Effect of Age

New counters could withstand around -30 V before breakdown. For new counters, the optimum voltage was around -5 V. As the counters aged, the optimum voltage increased to around -30 V. A two-year-old counter was recently tried and found to withstand a negative bias as high as -250 V.

4. Effect of temperature

The germanium counters used in these experiments and made by using Method I could detect particles only at low temperatures. They start detecting particles when the temperature reached about 77°K. Although the counters could withstand higher voltages at 77°K, they were not as stable as when used at helium temperatures. With aging, however, the counters were able to withstand much higher voltages at helium temperatures. Most of the counting runs on einsteinium and californium were made with a bias of -30 V.

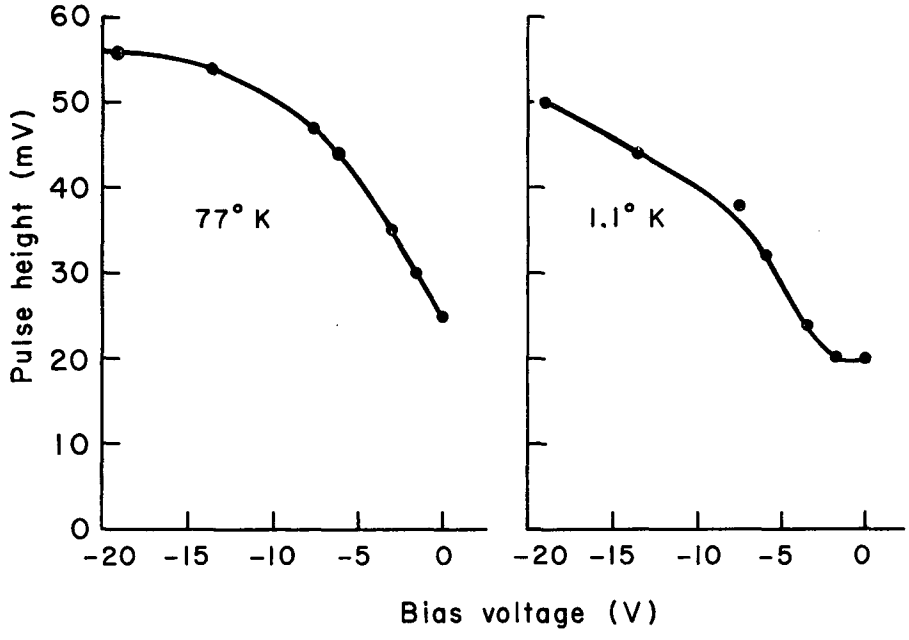

Fig. 5. Pulse height of alpha particles from an Am^{241} source as a function of applied bias voltage and temperature.

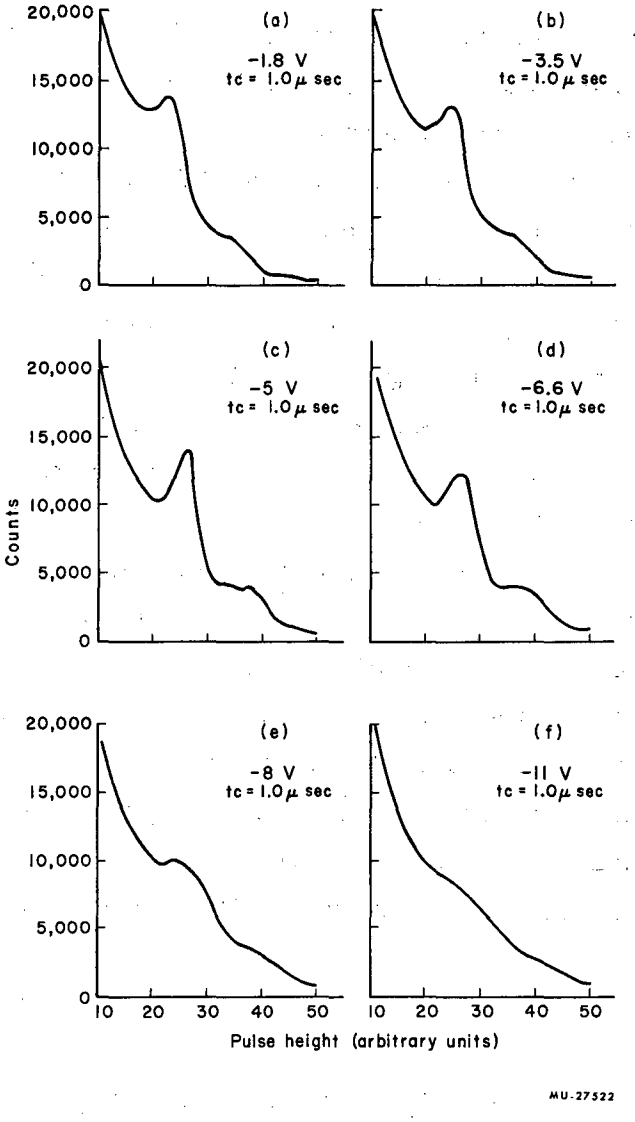

Fig. 6. Beta spectrum of Hg^{203} deposited on aluminized Mylar as a function of applied bias voltage, obtained by using an amplifier time constant (tc) of 1 μsec. Note the conversion lines.

The best resolution obtained with counters made by Method I was about 8% for the main alpha group of Am^{241}. For purposes of comparison, several alpha spectra are shown in Fig. 7. In Fig. 8a, the alpha spectrum from the Am^{241} source used in Fig. 7 was taken with a good resolution (about 22 keV full width at half-maximum) silicon guard-ring detector at room temperature. For comparison, the alpha spectrum from another Am^{241} source was taken with the same silicon guard-ring detector (Fig. 8b). The alpha spectrum from this source, taken with one of the germanium surface-barrier detectors at 77°K was very much similar to that of Fig. 7a; that is, the germanium counter was unable to separate the more-prominent alpha groups in Am^{241}.

A few surface-barrier silicon detectors made using Method II were also tried at 77°K. They could detect alpha particles when a bias voltage ranging from -600 to -1200 V was used. The pulse height obtained increased with increasing negative bias. However, after a few minutes of operation at the optimum potential, removal of the biasing voltage did not affect the pulse-height distribution. It took around 30 minutes, after removal of the biasing voltage, for the pulses to gradually diminish to noise level. Because of this polarization effect, the silicon detector was unsuitable for use in the nuclear-alignment experiments. When used at liquid-helium temperatures, the silicon surface-barrier detector operated only for a few minutes at best, and in most instances did not operate at all.

C. Bench Testing and Mounting of Counters

Each counter used for the detection of alpha particles from the einsteinium and californium samples was tested in a bench setup before mounting in the cage. The counters were then secured to the cage with a screw and nut. A length of insulated manganin wire was soldered to each of the terminal lugs on the counters with an alloy of zinc and cadmium. For the last experiment in einsteinium, collimators

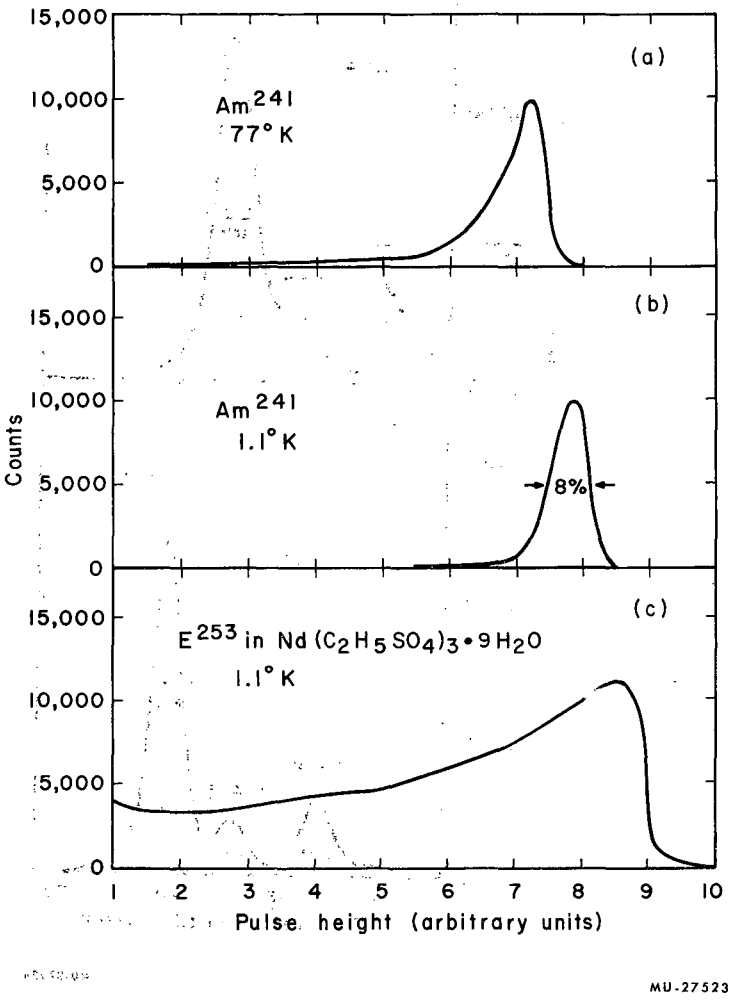

Fig. 7. Typical alpha-particle from (a) Am^{241} at 77°K, (b) Am^{241} at 1.1°K, and (c) E^{253} grown into a crystal of neodymium ethylsulfate . A germanium surface barrier counter was used.

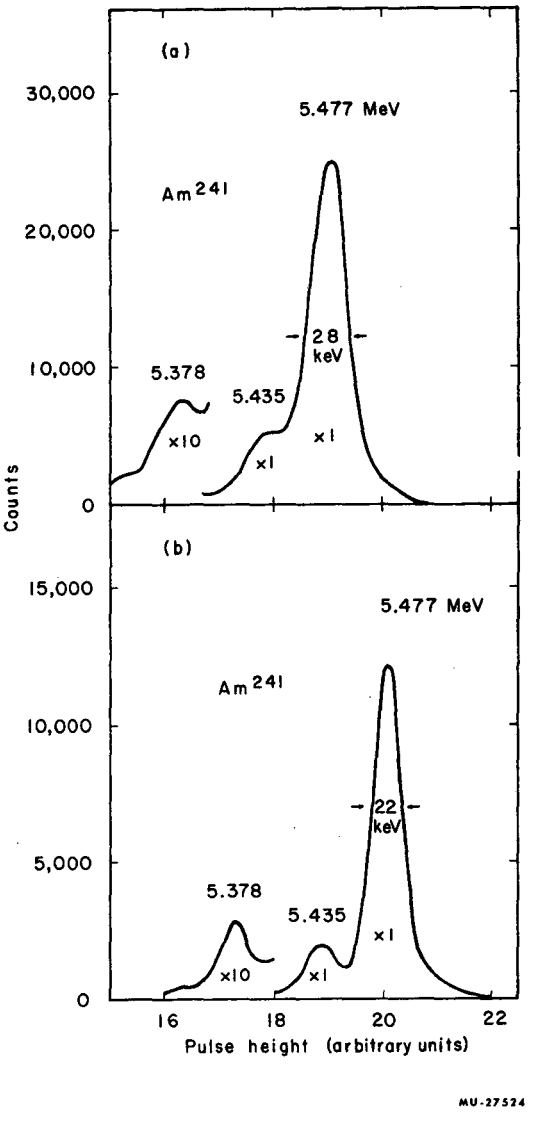

Fig. 8. Typical alpha-particle spectra from (a) a thin, collimated Am^{241} source and (b) the Am^{241} source used in Figs. 7 (a) and (b). A silicon-guard-ring detector was used at room temperature.

were used. These were secured by the same screws used for attaching the counters to the cage. Just before a run, the cage was attached to the cap K. When the counters were not in use, the whole cage was usually kept in a dessicator.

D. Summary

The procedure outlined in Method I produced counters which worked satisfactorily for counting beta and alpha particles at low temperatures. The counter mounting design met the requirements of limited space, thus making it possible to have several counters inside the cryostat. It should be noted, however, that the counter having its counting surface perpendicular to the magnetic field (during magnetization) was temporarily affected. When the counter was along the direction of the field, it was only slightly affected. Both counters, however, were restored to normal operation after demagnetization.

The germanium counters produced by Method I still counted after two years of operation. Counters made with plates cut supersonically did not detect particles. Silicon surface-barrier detectors also did not work satisfactorily at temperatures required for nuclear alignment.

Several points gathered from the experiments with the germanium counters must be emphasized:

(a) The resolution of the counters is very dependent on surface contamination. Counters that had been exposed to air did not operate even with the proper bias. However, this condition was usually temporary. The counters could be made to operate by applying a negative voltage exceeding the breakdown voltage or by putting forward bias on the counters. Counters "revived" in this manner tended to be noisy. When cleaned successively with ethylene trichloride, methanol, and deionized water, and drying in a stream of dry nitrogen gas, the counters could be restored to normal operating conditions.

(b) For best resolution, the amplifier time constant must be adjusted to the proper value. For very new counters, a time constant of 1 μsec gave the best resolution. As the counters aged, the time

constant required became shorter. The amplifier used in these experiments had equal differentiating and integrating time constants.

(c) The shielding of the signal leads before amplification should be excellent in order to get a good signal-to-noise ratio.

(d) Stray capacitance of the detecting system should be minimized to prevent too much signal attenuation. This is very important in the stage preceding the preamplifier.

This study is by no means comprehensive. Factors such as surface damage, bulk properties (carrier lifetime, resistivity) of the germanium single crystal, and types of impurities for doping the semiconductor were not studied. An investigation of these would greatly aid in determining the parameters needed for producing detectors with good resolution. The practicality of germanium detectors for nuclear-alignment work is demonstrated in this thesis. Although the resolution of the counters was not excellent, these counters were certainly far superior to other particle detectors in this type of investigation. It is hoped that the few data given here will aid in developing better germanium particle counters.

IV. EXPERIMENTAL PROCEDURE

A. Sample Preparation

1. Dysprosium

The dysprosium isotopes were obtained by bombarding natural gadolinium oxide powder (99.9% pure) with 48-MeV alpha particles accelerated at the Berkeley 60-in. cyclotron. This bombardment produced a mixture of Dy^{155} and Dy^{157}, the latter constituting the greater part of the activity.

The dysprosium fraction was purified and separated from the main Gd mass by the usual ion-exchange method, employing α-hydroxyisobutyric acid as eluant. The resulting Dy^{3+} isotopes were converted into the ethylsulfate and grown into a single crystal of $Nd(C_2H_5SO_4)_3 \cdot 9H_2O$. The sample was then ready for mounting.

2. Californium and Einsteinium

Californium and Einsteinium were obtained by neutron irradiation of curium isotopes.[7] The neutron-capture sequence is given by

$$
\begin{array}{ccccccc}
 & & & & & & E^{253} \\
 & & & & & & \beta^- \uparrow \\
 & & & & Cf^{249}(n,\gamma)Cf^{250}(n,\gamma)\cdots & & Cf^{253} \\
 & & & \beta^- \uparrow & & \beta^- \uparrow & \\
 & & & Bk^{249} & (n,\gamma) & Bk^{250} & \\
 & & \beta^- \uparrow & & & & \\
Cm^{244}(n,\gamma)Cm^{245}(n,\gamma)\cdots & & Cm^{249} & & & & .
\end{array}
$$

The Cf^{249} was obtained by isolating the berkelium fraction from the neutron-irradiated samples, and at a later date the daughter was recovered. Similarly the E^{253} was obtained by prolonged irradiation of curium samples with neutrons until Cf^{253} was produced. The einsteinium fraction was then chemically separated by ion-exchange methods.

The Cf^{3+} and E^{3+} ions adsorb on Dowex-50 cation resin and elute ahead of the first rare-earth element. The usual eluting agent is buffered alpha-hydroxyisobutyrate solutions. In some cases, 13M HCl in C_2H_5OH (20% by volume) was used in conjunction with the cation-exchange column. Both californium and einsteinium form anionic chloride complexes in 13M HCl and advantage was taken of this in separating these ions from the rare earths. The concentrated HCl was passed through an anionic resin, and the chloride complexes were adsorbed. The rare-earth ions that were not adsorbed passed through the column. Additional concentrated HCl solutions were then used to elute the complexes from the resin.[8]

In one stage of this experiment, it was necessary to recover tracer amounts of californium from several grams of neodymium ethylsulfate. The procedure followed was to decompose the ethylsulfate by prolonged heating. Then it was heated with a mixture of HNO_3 and HCl until a rose-colored residue was obtained on heating to dryness. The residue was then dissolved in concentrated HCl and adsorbed on Dowex-50 cation resin. The eluent solution was concentrated and passed through another cation column. The procedure was repeated several times until most the neodymium was removed. The resulting solution was again concentrated to a very small volume and passed through a Dowex-1 anion-exchange column. The activity was collected on platinum planchettes and evaporated to dryness. The dried spots were taken up in water and evaporated again to dryness.

The separated activity was then grown into a single crystal of neodymium ethylsulfate. A single crystal with a suitable crystal face was selected. Minute volumes (~ 0.005 cc) of an aqueous solution containing trivalent Cf^{249} or E^{253} were pipetted onto the selected spot and allowed to dry. This was repeated until an adequate amount of activity

was accumulated. The method proved to be practical and satisfactory as shown by the results of the experiments. It is interesting to note the ease with which the actinides substituted into the neodymium ethyl-sulfate lattice, thus demonstrating that the lanthanides and actinides are isomorphous in this salt.

After the spot had dried, the crystal was ready for mounting. The crystal containing the activity was fastened with Duco cement to a glass framework made of 2mm glass rod. This was attached to the assembly containing the manganous ammonium sulfate pill and glycerol-chrome alum slurry (see Fig. 2). The sample was mounted so that the active spot could be viewed by the two alpha counters.

B. Assembly of Apparatus

The counter assembly (Sec. IIE) was screwed in place, and the signal leads were soldered to the Kovar seals (L, L', Fig. 2). The sample assembly was next joined to the tungsten-glass supporting rod and adjusted as explained in the previous section. The position of the sample was measured for placement of the detecting coil (Sec. IIB). The sample chamber was soft-soldered to the cap K and coated with Aquadag (colloidal graphite). The Aquadag coating served to eliminate black-body radiation from parts of the apparatus that were above the temperature of the bath. The detecting coil was taped in place so that the upper secondary surrounded the sample.

The sample chamber was filled with helium gas at about 1.1 atm and then surrounded with a dewar containing liquid nitrogen. This precaution was taken so that the glycerol slurry, which could contain considerable amounts of dissolved air, did not bubble out when the pressure inside the chamber dropped as the apparatus was cooled to liquid-nitrogen temperature. When the system had come to equilibrium with the nitrogen bath, as indicated by an auxiliary manometer, the helium-gas supply line was shut off, and the inner chamber was evacuated by an oil-diffusion pump for several hours to partially degas all surfaces.

The final step in preparation for the actual experiment was the replacement of the nitrogen dewar with the liquid-helium dewar, which had been precooled to 77°K. The helium dewar was bolted in place, making sure that the rubber o-ring was properly seated. The liquid-nitrogen dewar was next hooked into position, and filled with liquid nitrogen. Then the helium dewar was filled with about 3 liters of helium.

C. Temperature Calibration

The actual experiments were begun with the calibration of the mutual-inductance system. A pressure of about 30μ of helium exchange gas was maintained in the sample chamber during the calibration. The vapor pressure of the helium bath was slowly decreased by pumping. The mutual inductance of the detecting coil as the sample cooled was recorded and plotted against the reciprocal of the absolute temperature as obtained from the known vapor pressure-temperature curve of liquid helium. The points obtained described a straight line (because the salt follows Curie's law: $\chi \propto 1/T$), from which a relationship could be obtained for determining the "magnetic temperature" T^* reached upon adiabatic demagnetization of the sample. The magnetic temperatures reached after demagnetization were converted into absolute temperatures by using the work of H. Meyer.[9]

D. Counting Runs

1. Dysprosium

In this experiment only the angular distributions of the emitted gamma rays were determined. A more convenient setup was used. It was identical in most respects to the apparatus described above except for the sizes of the dewars and the sample chamber.

The sample was magnetized along the crystalline c-axis. Alignment was obtained by cooling the crystal by adiabatic demagnetization.

By demagnetizing from different fields extending up to 18 kG, temperatures from 1.1°K (the helium-bath temperature) down to 0.02°K were obtained. Gamma-ray intensities at different temperatures were recorded by two counters: one parallel to the crystalline c-axis and another perpendicular to it. The intensity distributions of the gamma rays were also determined at a series of angles θ from the crystalline c-axis at the lowest temperatures attained. During and immediately following the gamma-ray counting, the mutual inductance of the sample was monitored. Counting was usually started within a few seconds after demagnetization.

The gamma-ray intensity was normalized to the (isotropic) intensity at 1.1°K by warming the crystal to the bath temperature by admitting helium gas into the sample chamber. When the cyrstal had warmed, a normalization count was taken for the same length of time. Corrections were made for half life, blocking time, solid angle, and background due mostly to Tb^{155}, the daughter of Dy^{155}, which has an anisotropy of opposite sign.[10]

2. Einsteinium

Since no prominent gamma rays follow the alpha decay, this was purely an alpha experiment. The alpha particles emitted from the crystal, cooled by adiabatic demagnetization from different fields, were continuously counted by two detectors (at 0 and 90 deg from the crystalline c-axis) until the sample had warmed to the bath temperature. However, only the counts obtained immediately after demagnetization were used in the calculations. Normalization counts were also done as above. Blocking-time was automatically corrected for by the pulse-height analyzer. Corrections for solid angle were made by measurement of the counter dimensions and distances. A final run was made at the lowest temperatures attainable, using collimators for which solid angle corrections were small and precisely known.

3. Californium

Californium-249 has two prominent gamma rays, and alpha particles and gamma rays were counted simultaneously. Both the gamma-ray counters

and the alpha counters were placed at 0 and 90 deg from the crystalline c-axis. The four counters were started at the same time and the inductance of the sample was monitored. Because of the low intensity of the californium sample, the gamma-ray counters were shielded with thick sheets of lead to minimize background effects. Corrections for solid angle were made as in the einsteinium procedure. The gamma-ray anisotropies were also corrected for background and solid angle. The sample was not collimated.

V. THEORY OF NUCLEAR ORIENTATION

A. The Spin Hamiltonian

In order to produce nuclear orientation, one must resolve the degeneracy of the nuclear spin I_0 of the nucleus to be oriented into its component substates M, ($M = +I_0, I_0-1, \ldots, -I_0$), each possessing an energy E(M). The separation is accomplished by application of magnetic or inhomogeneous electric fields. The relative position and energy of separation between various substates is determined by the interactions that resolve the $(2I_0 + 1)$-fold spin degeneracy. The population of each substate for a system of independent nuclei in thermal equilibrium is governed by the Boltzmann function

$$a_M = C \exp\left(\frac{-E(M)}{kT}\right) . \qquad (1)$$

At temperatures where all substates are equally populated, i.e. where we have $[E(M) - E(M+1)] \ll kT$, the nuclear orientation is random. Therefore one must induce preferential population of some substates in order to produce some degree of nuclear orientation. If the energy separation between the lowest substate and the next higher sublevel is sufficiently large, complete nuclear orientation is accomplished at a relatively high temperature. This low temperature method is the one employed in these experiments. Optical pumping and microwave methods can also be used in some cases.

The most obvious way of separating the nuclear substates is to apply a strong external magnetic field. Another method utilizes the intense internal crystalline fields present in paramagnetic salts or a combination of the two. The action of an external magnetic and internal crystalline fields cause the separation in energy of the normally degenerate levels of a free ion. If such an ion is incorporated in a paramagnetic crystal possessing axial symmetry about the z-axis, the interaction can be expressed (assuming no collective effects) by a spin Hamiltonian of the form[11]

$$\mathcal{H} = \beta[g_{\parallel} H_z S_z + g_{\perp} (H_x S_x + H_y S_y)] + D[S_z^2 - \tfrac{1}{3} S(S+1)] - \left(\frac{\mu_N}{I_0}\right) \vec{H} \cdot \vec{I}$$

$$+ \Delta_x S_x + \Delta_y S_y + A S_z I_z + B(S_x I_x + S_y I_y) + P [I_z^2 - \tfrac{1}{3} I_0 (I_0 + 1)] , \qquad (2)$$

where β is the Bohr magneton, μ_N is the nuclear magnetic "dipole" moment, $g_{\parallel}$ and $g_{\perp}$ are ionic g-factors parallel and perpendicular to the field, respectively; S is the effective electron spin, and $\Delta = (\Delta_x^2 + \Delta_y^2)^{1/2}$.

The effective electron spin S is obtained by setting the multiplicity of the electronic levels equal to $(2S+1)$. Thus, for a doubly degenerate level, the effective electronic spin is $1/2$. Incidentally, if this is the case, the D term drops out in the expression for the spin Hamiltonian of the lowest doublet.

The first term in the Hamiltonian represents the splitting of the electronic levels by an external magnetic field. The third term corresponds to the direct interaction of the nuclear magnetic "dipole" moment μ_N with the external field. If no external magnetic fields are applied, these drop out. The term in D represents the splitting of the electronic levels by the electric field. The P term is the interaction of the nuclear quadrupole moment Q with the crystalline electric-field gradient. The A and B terms are responsible for hfs splitting and are due to the interaction of the nuclear moment with the magnetic field created at the nucleus by unpaired electrons. The term in A or B vanishes according as $g_{\parallel}$ or $g_{\perp}$ vanishes, if the electronic angular momentum J is a good quantum number. The term in Δ represents the effect due to departures from the symmetry assumed for the crystalline electric field. This term is assumed to have a gaussian distribution centered around zero. One or more of the terms in the spin Hamiltonian may be needed to evaluate

the experimental data. One must also take account of any other interactions that may be present.

To obtain the energy eigenvalues, one must solve the Schroedinger equation

$$\mathcal{H}\psi(M) = E(M)\psi(M) , \tag{3}$$

where $\psi(M)$ denotes the wave function describing the substate M. To facilitate the solution of the above equation for rare-earth ions, Elliott and Stevens introduced the notion of operator equivalents.[11-14] For the rare-earth ions in crystals possessing anisotropic crystalline fields ($Nd(C_2H_5SO_4)_3 \cdot 9H_2O$ in the present experiments), Elliott and Stevens give

$$A = 4\,\beta\beta_N\,\mu_{\frac{N}{I_0}}\,\langle r^{-3}\rangle\,\langle +|N_z|+\rangle , \tag{4a}$$

$$B = 4\,\beta\beta_N\,\mu_{\frac{N}{I_0}}\,\langle r^{-3}\rangle\,\langle +|N_x|-\rangle , \tag{4b}$$

and

$$P \cong -\frac{9e^2Q}{4I_0(2I_0-1)}\,\langle r^{-3}\rangle\,\langle J||\alpha||J\rangle\,\langle +|J_z^2 - \tfrac{1}{3}J(J+1)|+\rangle , \tag{4c}$$

where $\langle +|N_z|+\rangle$, and $\langle +|N_x|-\rangle$ are the diagonal and nondiagonal (within the ground doublet) matrix elements of the tensor describing the magnetic hyperfine structure, $\langle J||\alpha||J\rangle$ and $\langle +|J_z^2 - \frac{1}{3}J(J+1)|+\rangle$ are matrix elements which are diagonal in J and J_z and describe the quadrupole hyperfine-structure interaction, and J and J_z are the total ionic angular momentum and its component. The factor

$\langle r^{-3} \rangle$ is the expectation value for the 4f electrons, and β_N is the nuclear magneton. The other quantities have their usual significance.

Values of $\langle r^{-3} \rangle$ for the rare-earth ions have been calculated by Judd and Lindgren,[15] and the elements of the matrices involved have been evaluated by Elliott and Stevens.[11-14] The operator equivalents have been calculated on the assumption that Russell-Saunders coupling holds for the rare-earth ions. It is seen clearly from the above equations that if, for a particular ion, the factors AI_0/μ_N, or BI_0/μ_N, and PI_0/Q have been evaluated or experimentally determined for one isotope, the nuclear magnetic moment and the quadrupole moment for another isotope can be obtained by comparison of the experimental data with the above factors, provided the spin I_0 is known. The latter may also be obtained by a careful analysis of the data, as will be shown below.

B. Angular Distribution of Gamma Rays from Aligned Nuclei

The angular distribution of gamma rays from aligned nuclei is given by[16]

$$W(\theta) = 1 + B_2U_2F_2P_2(\cos\theta) + B_4U_4F_4P_4(\cos\theta) + \ldots \qquad (5)$$

where the B_k's are orientation parameters. The U_k's are a measure of the amount of reorientation which occurs during any unobserved preceding transitions. The functions F_k are dependent upon the angular momenta involved in the observed transition and are similar to the F_k's in angular correlation theory. The function $P_k(\cos\theta)$ is the Legendre polynomial of order k. The k's span even integers because of the symmetrical nature of alignment, whereby parallel and antiparallel senses of orientation of the nuclear spin component I_z possess the same energy. The functions also decrease very rapidly as k increases and, in cases of low degrees of orientation, terms in k = 2 are sufficient to describe the distribution.

The evaluation of the functions U_k and F_k can be best described by using the following decay sequence as an example:

$$I_0 \xrightarrow{L_1} I_1 \xrightarrow{L_2} I_2 ,$$

where I_0 is the nuclear spin of the oriented nucleus, L_1 is the angular momentum of the unobserved radiations, I_1 is the spin of the state from which the observed radiation with angular momentum L_2 originates, and I_2 is the spin of the state resulting after emission of radiation L_2. For the above decay sequence, the functions are given by

$$U_k = [(2I_0+1)\ (2I_1+1)]^{1/2}\ (-1)^{I_0+I_1-L_1}\ W(I_0I_0I_1I_1;\ k\ L_1) \qquad (6a)$$

$$F_k = (-1)^{I_2-I_1-1}\ (2I_1+1)^{1/2}\ (2L_2+1)$$

$$\times\ C(L_2L_2k;\ 1\ -1)\ W(I_1I_1L_2L_2;\ k\ I_2) \qquad (6b)$$

where $W(abcd;\ ef)$ is a Racah coefficient and $C(ABC;\ \beta\gamma)$ is a Clebsch-Gordan coefficient.

If the unobserved preceding transition is a mixed transition with a mixed component L_1' of amplitude δ, U_k is replaced by

$$U_k = \frac{U_k(L_1) + \delta^2\, U_k(L_1')}{(1 + \delta^2)} . \qquad (7)$$

If there are more than one unobserved preceding transitions, the effective U_k is given by the product of the U_k's for each transition, all corrected for any admixtures.

If the observed transition is a mixture of L_2 and L_2' radiations, the effective F_k is given by

$$F_k = \frac{F_k\,(L_2 I_2 I_1) \;+\; \delta^2 F_k (L_2' I_2 I_1) \;+\; 2\delta F_k\,(L_2 L_2 I_2 I_1)}{(1+\delta^2)} . \qquad (8)$$

The term in 2δ represents the interference term between the L_2 and L_2' components. The factor δ^2 is called the mixing ratio. Note that the interference term in the U_k vanishes. Values of the F_k functions have been tabulated by Ferentz and Rosenzweig.[17]

C. Orientation Parameters

The orientation parameters can be represented as

$$B_k = (2k+1)^{1/2} \sum_M C(I_0 k I_0;\ M\ 0)\ W(M), \qquad (9)$$

where again M is the magnetic quantum number of the oriented nucleus, k is even and spans the value 0 to $2I_0$ or $2L_1$, whichever is smaller, and we have

$$W(M) = \exp\,[-E(M)/kT] \Big/ \sum_M \exp\,[-E(M)/kT] = a_M \Big/ \sum_M a_M . \qquad (10)$$

Energies E(M) are obtained by solving Eq. (3). In these experiments, the interaction is adequately expressed by (see Discussions)

$$\mathcal{H} = AS_zI_z \,, \tag{11}$$

where B_k becomes a function of a single parameter $\beta = A/2kT$. Values of β for different spins I_0 have been calculated for the different B_k's for the case of an effective spin $S = 1/2$.[18] From the temperature dependence of the anisotropy which is proportional to $B_kU_kF_k$, a comparison with a plot of B_k as a function of β will yield a value A', since U_kF_k can be evaluated from the assumed transition. A comparison of A' with Eq. (4a) yields the nuclear moment μ_N. Conversely, if A [that is, E(M)] is known, U_kF_k can be evaluated and the decay sequence established.

One immediate conclusion that can be drawn from the above discussions is that the angular distribution is isotropic for a system of nuclei with spin 0. Isotropic distribution also results for spin 1/2, since this leads only to a term with $k = 1$, that is, no nuclear alignment. Whenever the observed transition is preceded by an intermediate state with spin 1/2 or zero, isotropic distribution will result. In the case of spin 1/2 for the oriented nuclei, another kind of orientation results. This is termed nuclear polarization, and only a term in B_1 appears. Polarization is orientation in both sense and direction, that is, the substate with quantum number + 1/2 has an energy different from the substate characterized by - 1/2.

VI. NUCLEAR ALIGNMENT OF DYSPROSIUM-155 AND DYSPROSIUM-157

A. Results

The two most intense gamma rays, at 327 and 227 keV, had anisotropic distributions. These have been shown to belong to the decays of Dy^{157} and Dy^{155}, respectively, by Toth and Rasmussen,[19] Toth and Nielsen,[20] and Mihelich et al.[21] No other gamma rays were examined for anisotropy, as these two were the only prominent ones.

A typical spectrum is shown in Fig. 9. The anisotropy, $\epsilon = 1 - [W(\frac{\pi}{2})/W(0)]$, of the 327-keV γ-ray of Dy^{157} plotted against $1/T$ is shown in Fig. 10. The 227-keV γ-ray anisotropy is shown in Fig. 11. The intensity distribution of the 327-keV γ-ray as a function of the angle θ between the directions of propagation and the crystalline c-axis is shown in Fig. 12.

The experimental angular distributions at $T = 0.022^{\circ}K$ were found to follow

$$W(\theta) = 1 + (0.108 \pm 0.008)\, P_2 (\cos\theta)$$

and

$$W(\theta) = 1 + (0.060 \pm 0.025)\, P_2 (\cos\theta)$$

for the 327 and 227-keV γ-rays, respectively.

In this experiment only terms in k=2 in the angular distribution were necessary for treating the data. To calculate the orientation parameter, one must know the exact form of the spin Hamiltonian. How this is arrived at is explained below.

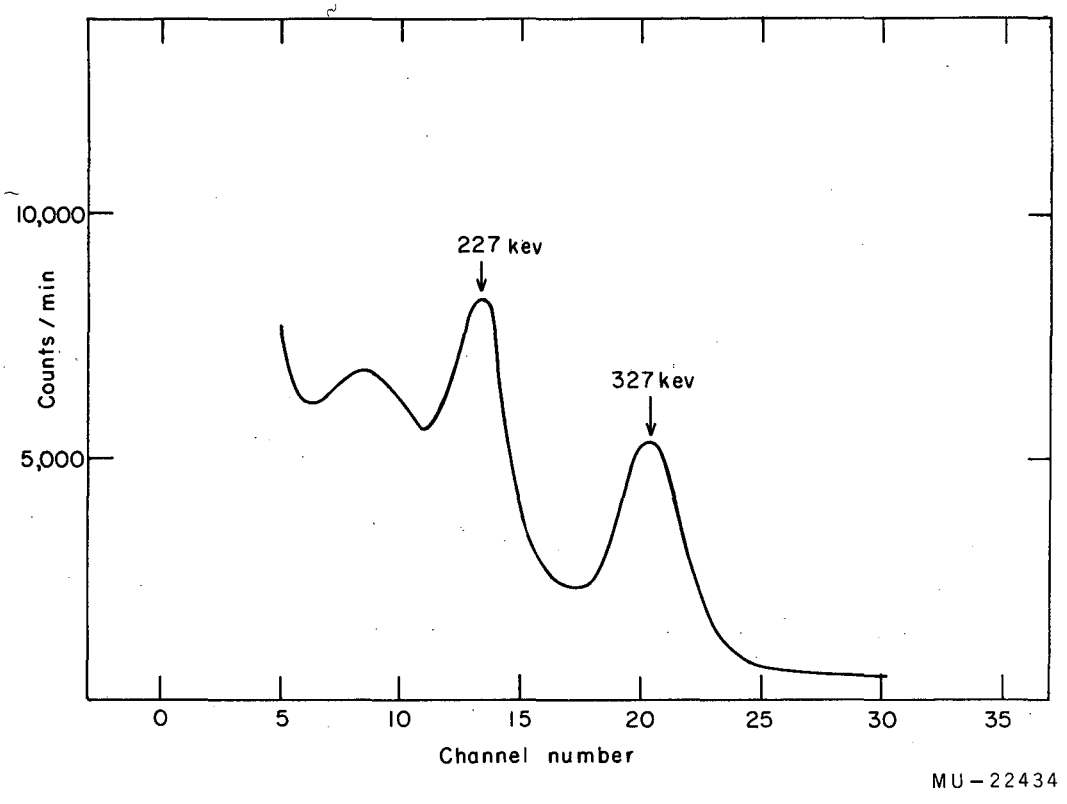

Fig. 9. Typical γ-ray spectrum of a Dy^{155} and Dy^{157} mixture.

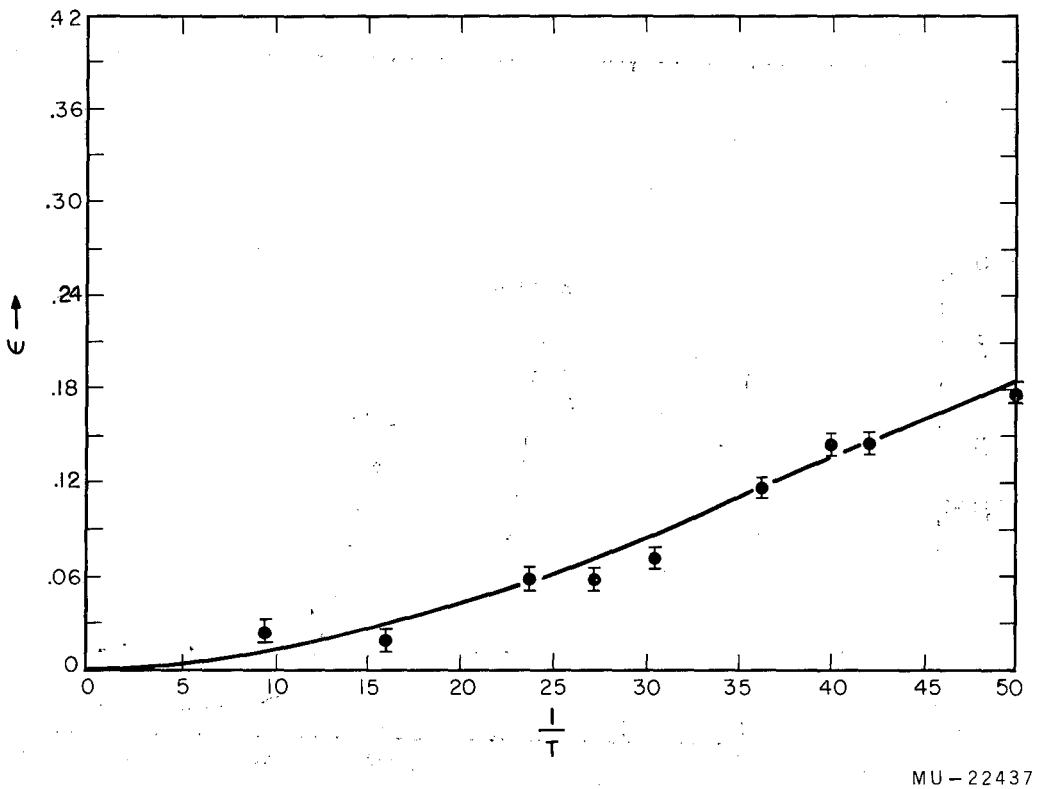

Fig. 10. Anisotropy of the 327-keV γ ray of Tb^{157} as a function of 1/T.

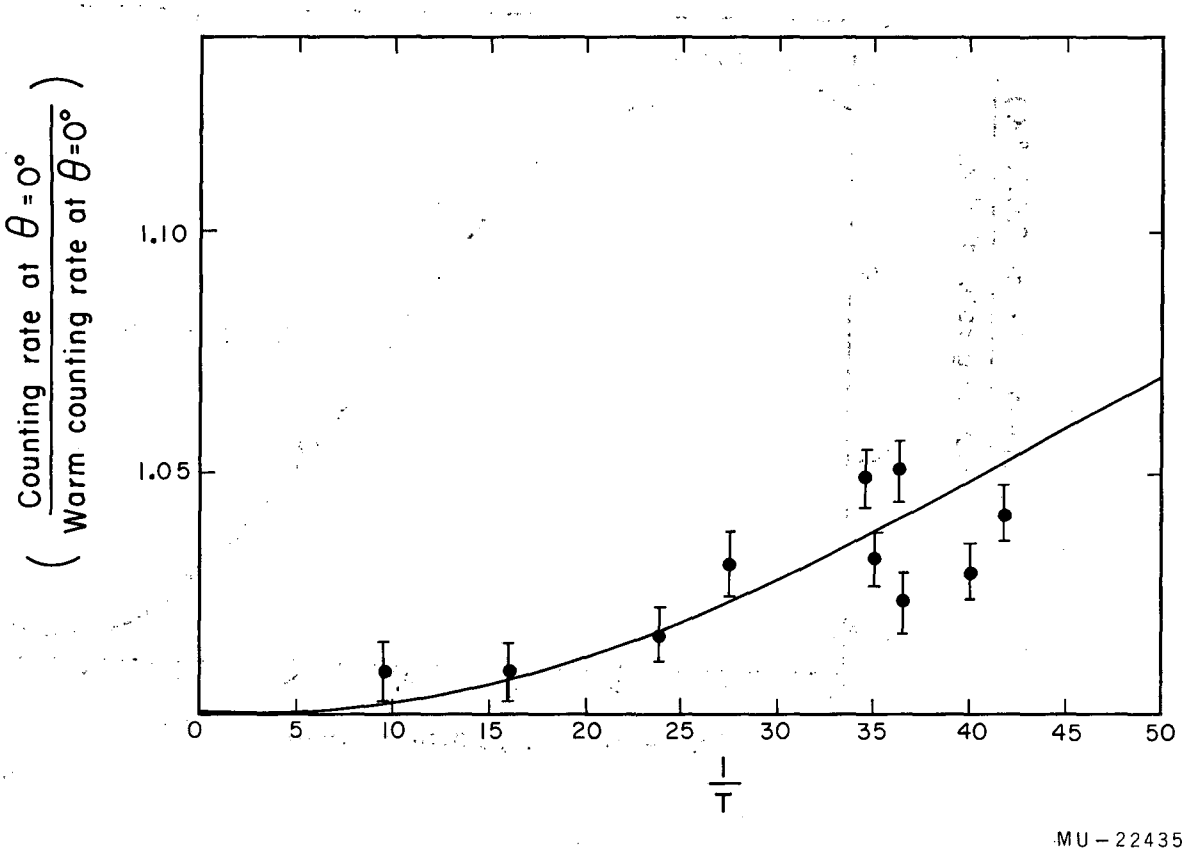

Fig. 11. Plot of $B_2U_2F_2$ for the 227-keV γ ray of Tb^{155} vs 1/T.

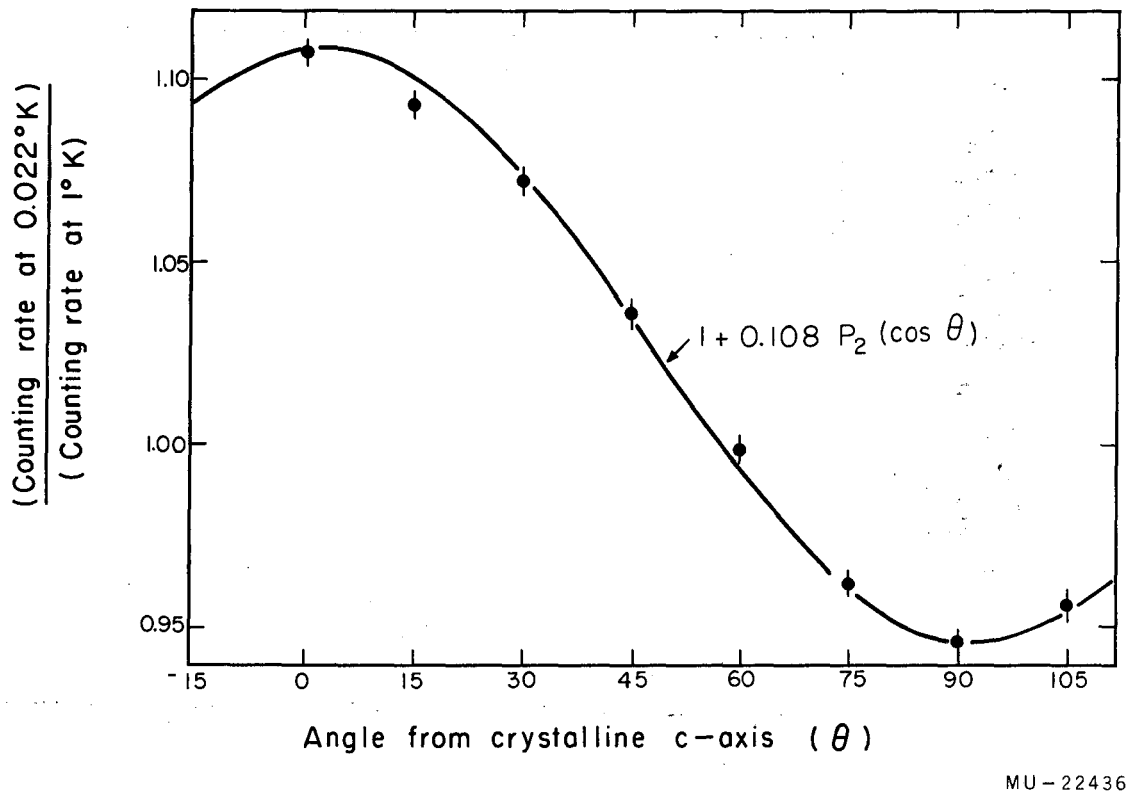

Fig. 12. Intensity distribution of the 327-keV γ ray of Tb^{157} at 0.022 °K.

B. Discussion

Tripositive dysprosium has the configuration $4f^9$. The ground level, $^6H_{15/2}$, is split into doublets by the interaction of the electronic charge of the 4f electrons with the crystalline electric field. These doublets may be characterized in the first approximation by $|\pm J_z\rangle$. It was shown that there are two possible ground doublets:[22] (a) a doublet which is mostly $|\pm 9/2\rangle$ with some admixtures of $|\mp 3/2\rangle$ and $|\mp 15/2\rangle$, and (b) another doublet composed of a mixture of the states $|\pm 7/2\rangle$ and $|\mp 5/2\rangle$.

The first doublet has $g_\perp = 0$ and $g_\parallel = 10.3$, while the second has $g_\perp \approx g_\parallel$. Paramagnetic resonance has shown that resonance is observed at $14^\circ K$,[23] but not at helium temperatures.[24] This may be interpreted as evidence that the (nonresonant) doublet (a) lies lowest. This interpretation was confirmed by susceptibility measurements at helium temperatures,[25] which give for the ground doublet $g_\parallel = 10.76 \pm 0.1$ and $g_\perp = 0$.

Because we have $g_\perp = 0$, the effective spin Hamiltonian can be expressed by Eq. (11). Using Eq. (4c), we see that the quadrupole interaction should have negligible effect on the nuclear alignment for the assumed ground doublet.

The decay scheme of Dy^{157} has been established fairly well, and the portion of interest in this investigation is shown in Fig. 13. According to the notation of Mottelson and Nilsson,[26] the ground-state assignment for Dy^{157} is 3/2 - [521]. The 227-keV γ-ray has been found to have multipolarity E1. Just as in the case discussed below for Tb^{155}, if the ground-state spin and parity of Tb^{157} are 3/2 +, then the sign and magnitude of the γ-ray anisotropy preclude any assignment other than 5/2 - for the 327-keV state. For the spin sequence 3/2-(L=1) 5/2 - (E1) 3/2 +, one can calculate U_2F_2 using Eq. (5a,b). This gives for the theoretical intensity distribution of the 327-keV γ-ray

$$W(\theta) = 1 + 0.280\, B_2P_2\,(\cos\theta). \qquad (12)$$

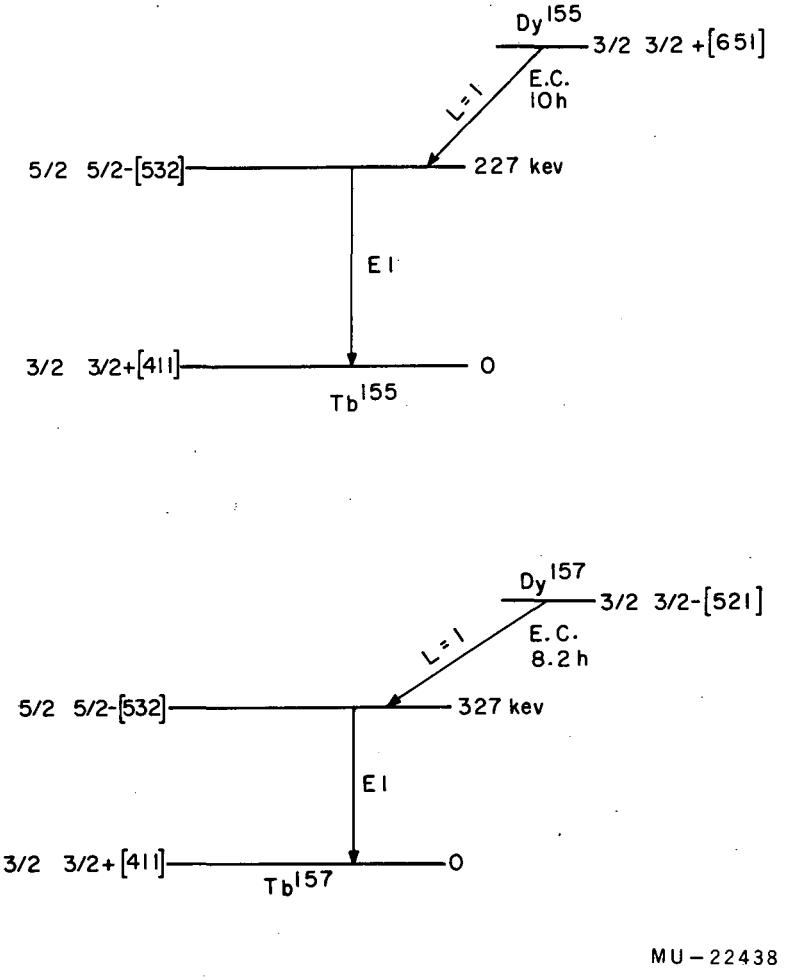

Fig. 13. Partial decay schemes of Dy^{155} and Dy^{157} relevant to this experiment.

For Dy^{155}, the decay scheme is not so comprehensive, but these results can be used to assign spin 5/2 - to the 227-keV level of Tb^{155} on the following arguments. Toth and others have assigned a spin of 3/2 + to the ground state of Tb^{155} and have shown that the 227-keV γ-ray is E1.[19,20] Thus the 227-keV state must have spin and parity 1/2-, 3/2-, or 5/2-. But a spin of 1/2-would allow no anisotropy in this γ-ray, while a spin of 3/2-would require $F_2 = -0.40$, which would produce an anisotropy with sign opposite to that experimentally observed. Thus only a spin and parity assignment of 5/2- for this level is compatible with the experimental data. Again for the spin sequence 3/2+ (L=1) 5/2- (E1) 3/2 + , the theoretical intensity distribution of the 227 keV γ-ray is given by Eq. (12).

From the temperature dependence of the anisotropy, the value of $|A'|$ can be obtained and compared with the expression for A obtained from Eq. 4a. The results are

$$\left|\frac{A'}{k}\right|_{157} = 0.048 \pm 0.003^{\circ}K$$

and

$$\left|\frac{A'}{k}\right|_{155} = 0.032 \pm 0.008^{\circ}K \ .$$

From Eq. (4a) and subsequent discussions, we obtain for Dy^{3+},

$$\frac{A}{k} = 0.227 \left(\frac{\mu}{I_0}\right)^{\circ}K \ . \qquad (13)$$

A comparison of Eq. (13) with the experimentally determined value $\left|\frac{A'}{k}\right|$ (k is the Boltzmann constant) yields for the nuclear moments in nuclear magnetons (n.m.)

$$\left|\mu_{157}\right| = 0.32 \pm 0.02 \text{ n.m.}$$

and

$$\left|\mu_{155}\right| = 0.21 \pm 0.05 \text{ n.m.}$$

Wide limits of error have been given for Dy^{155} because of the uncertainty in the background correction for the 227 keV γ-ray.

By using the values 0.28 and 0.32, respectively, for the deformation parameter δ and the gyromagnetic ratio of the core g_R given by Nilsson and Prior,[27] theoretical values of the magnetic moments of the two isotopes may be calculated. These are given in Table I based on ground-state assignments similar to those of the isotonic Gd isotopes,[28] together with the present experimental results and the known magnetic moments of Gd^{155}. It seems reasonable to infer that the signs of the magnetic moments of both Dy^{155} and Dy^{157} are negative. Then the magnitude may be compared with those calculated theoretically. In all these cases the theoretical magnitudes are too large, quite outside of experimental error. Thus, although the theory provides a good approximation to the magnetic moments, exact agreement is not obtained. The discrepancy may presumably be attributed to second-order effects, such as polarization of the core by the odd particle, which have not been included in the theory. Rasmussen and Chiao[31] have shown that the theoretical magnetic moments of several deformed nuclei may be brought into better agreement with experiment by assigning quenched g factors for the intrinsic spin of the odd particle. We note that use of quenched g factors for the odd neutron in Dy^{155} and Dy^{157} would improve the agreement between experiment and theory.

Table I. Comparison of theoretical and observed nuclear moments of dysprosium and gadolinium

Isotope	Ground state	μ(theory) $\delta = 0.28$ $g_R = 0.32$ (n.m.)	μ (observed) (n.m.)	Reference
Dy^{155}	$\frac{3}{2}$ + (651)	- 0.33	$\lvert 0.21 \pm 0.05 \rvert$	This work
Dy^{157}	$\frac{3}{2}$ - (521)	- 0.49	$\lvert 0.32 \pm 0.02 \rvert$	This work
Gd^{155}	$\frac{3}{2}$ - (521)	- 0.49	- 0.30	Ref. 29
			-0.30 ± 0.05	Ref. 30[a]

[a] Corrected for $\langle r^{-3} \rangle = 48.5 \text{Å}^{-3}$ (cf. Ref. 15).

VII. ANGULAR DISTRIBUTION OF ALPHA PARTICLES FROM ORIENTED NUCLEI

A. General Survey

With certain modifications, the theory of angular distribution of gamma rays from oriented nuclei can be applied to alpha-particle distributions. However, it is simpler to develop a separate treatment for this. It should be pointed out that in order to obtain nuclear alignment, the emitting nuclei must have nuclear spin $I_0 \geq 1$. Thus it cannot be applied to even-even alpha emitters. The present experiment involves the isotopes E^{253} and Cf^{249}.

A study of the angular distribution of alpha particles from oriented nuclei is of interest in determining the effect of angular momentum and the conditions at the nuclear surface. Aside from the effect of angular momentum, which is purely geometrical and can be treated quite independently, the distribution is dependent on physical parameters such as the hfs splitting and the branching to the different energy levels. The latter is of particular importance, since it reflects the conditions at the nuclear surface. In particular, the partial-wave intensities are governed by the ease with which the alpha particles can penetrate the barrier and the initial distribution of the alpha particles at the nuclear surface.

Spiers pointed out that if there are angular-momentum changes involved during alpha-particle emission, an anisotropic distribution of the emitted particles would be expected if the emitting nuclei were aligned.[32] In 1953, Hill and Wheeler predicted that, for a prolately deformed nucleus, the barrier against alpha emission is both lower and thinner at the poles or "tips" than at the equator or "waist" of the spheroid.[33] This can be seen quite readily by considering the diagram of the coulomb potential shown in Fig. 14.

The semiminor and semimajor axes of the spheroidal nucleus are given by r_0 and r_0', respectively. An alpha particle of kinetic

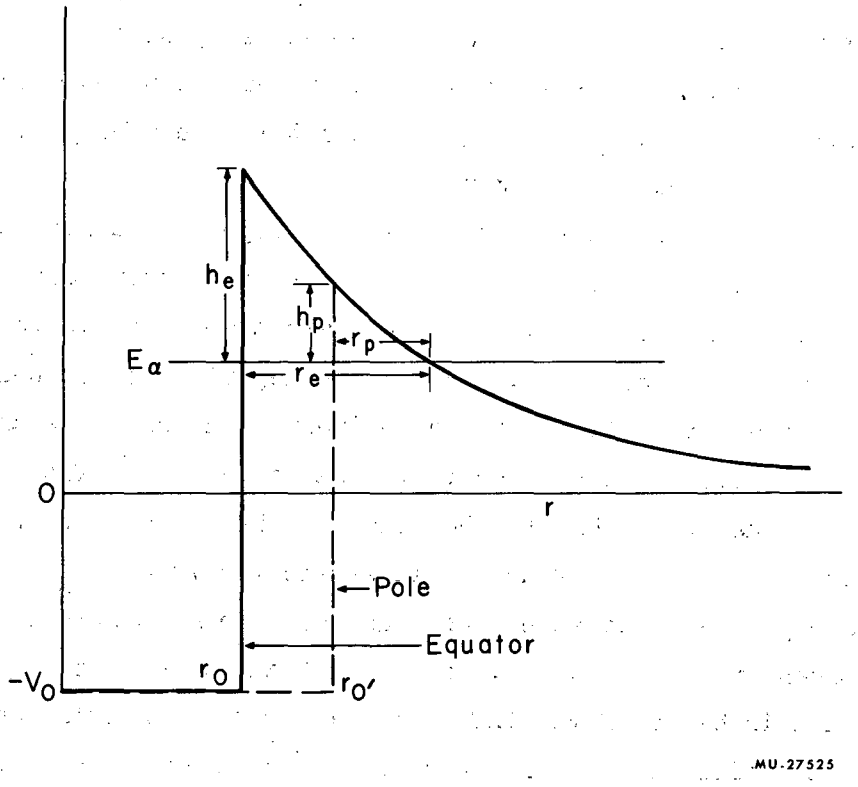

Fig. 14. Coulomb potential along the "tips" and "waist" of a spheroidal nucleus.

energy E_α within the potential well will have to penetrate a distance r_e along the equator or overcome the barrier height h_e. However, the alpha particle of the given kinetic energy will only have to penetrate the distance r_p along the tips, which is very much smaller. The barrier height h_p is also very much lower along the polar regions. Provided that there is a uniform probability of alpha-particle formation at the nuclear surface, enhanced alpha emission would in general be expected from the polar regions, and this could be proved through nuclear-alignment experiments.

The only experimental results reported so far on oriented alpha emitters were those of Dabbs and Roberts on uranium and neptunium.[34-37] In Np^{237} they observed enhanced alpha emission in the direction perpendicular to the crystal's c-axis. They also determined the sign of P as positive. In earlier experiments, the hfs constant A has been found to have a sign opposite to that of P.[38,39] With the above sign of P, they were able to show that at the temperature range studied, there is an excess of nuclei in states for which $I_z = \pm 1/2$. Eisenstein and Pryce have suggested that the O-U-O and O-Np-O bonds are of predominantly σ character, requiring P and Q to have opposite sign.[40] Upon this basis, Pryce inferred that $P > 0$ is evidence for $Q < 0$.[41] The positive sign of P obtained by Dabbs and co-workers would then lead to an oblate shape for Np^{237}, and the barrier in this case would be weaker in the "equatorial" region. This shape would conflict with the expectations of nuclear systematics. By assuming a model for the electronic structure of uranyl-like ions, which included the effects of P-π bonding, Roberts and Dabbs were able to reconcile the positive sign of P with a positive sign of Q.[42] The Np^{237} nucleus would then be prolate, and in the temperature range studied, alignment of the nuclear angular-momentum vector would be in the direction perpendicular to the crystalline c-axis. The observed enhancement of alpha emission in this direction would then be consistent with the Hill-Wheeler prediction.

B. Angular Momentum Effects in Alpha-Particle Distribution from from Oriented Nuclei

Rose has developed a general theory of angular momentum effects in alpha emission and expressed the results in terms of nuclear matrix elements.[43] The distribution is expressed as

$$W(\theta) = \sum_{L} A_{LL'} \sum_{k} G_k (T)\, C(LL'k;\, 00)\, W(I_0 I_0 LL';\, kI')\, P_k (\cos\theta), \tag{14}$$

where $C(LL'k;\, 00)$ and $W(I_0 I_0 LL';\, kI')$ are the Clebsch-Gordan and Racah coefficients, respectively. The initial nuclear spin is I_0, and I' gives the final spin of the nucleus; L is the angular momentum of the alpha particle; $P_k (\cos\theta)$ is the Legendre polynomial of order k; k is even and spans the value 0 to $2L$, $L+L'$, or $2I_0$, whichever is smaller. Thus for $I = 7/2$, we have $k = 0, 2, 4, 6$. However, terms for $k > 2$ may not be observed at high temperatures where $G_{k>2} \ll G_2$. For mixed and pure multipolarities, we have

$$A_{LL'} = \pm (A_{LL} A_{L'L'})^{1/2} \cos\phi_{LL'}$$

and (14a)

$$A_{LL} = a_L (2L + 1),$$

where a_L is the relative intensity of the Lth partial wave, and $\phi_{LL'}$ is the relative phase between the L and L' partial waves.

The term in G_k measures the alignment and is given by

$$G_k = \frac{\mathrm{Tr}\,(T_{k0}\, e^{-\mathcal{H}/kT})}{\mathrm{Tr}\,(e^{-\mathcal{H}/kT})}\,, \tag{15}$$

where $\mathcal{H}$ is the Hamiltonian responsible for the alignment, and T_{k0} is an element of an irreducible tensor. In particular, we have

$$T_{00} = (2I_0 + 1)^{-1/2} \tag{16a}$$

$$T_{20} = \left[\frac{180(I_0-2)!}{(2I_0+3)!}\right]^{1/2} \left[I_z^2 - \tfrac{1}{3}\, I_0\,(I_0+1)\right], \tag{16b}$$

and

$$T_{40} = 210\left[\frac{(2I_0-2)!}{(2I_0+5)!}\right]^{1/2}\left\{I_z^4 - \frac{1}{15}\left[3I_0^2\,(I_0+1)^2 - I_0(I_0+1)\right]\right.$$

$$\left. - \tfrac{1}{7}\left[6I_0(I_0+1) - 5\right]\left[I_z^2 - \tfrac{1}{3}\, I_0\,(I_0+1)\right]\right\}. \tag{16c}$$

Unlike the emission of gamma rays, in which there is no appreciable interference between the waves of different multipoles except E2 and M1 radiations, there is considerable mixing between different alpha waves leading to the same state. The relative phases of these waves enter into the angular distribution through Eq. (14a), and in the case of $L = 0$, 2 waves, may be determined immediately from the observed anisotropy. However, it may not be possible to

determine the relative phases of higher multipoles, since contributions due to these are likely to be small. Brussard and Tolhoek pointed out that it is mainly through the sign of the $a_0 a_2$ term that information can be obtained about the distribution of the nascent alpha particle on the nuclear surface.[44] The argument is as follows.[45] The wave function ψ_α describing the nascent alpha particle on the nuclear surface can be written as a series of Legendre polynomials in the body-fixed coordinate system:

$$\psi_\alpha = \sum_{k=0}^{2I_0} b_k P_k (\cos\theta') , \qquad (17)$$

where θ' is the polar angle in the body-fixed system. If we consider only the first two terms, the distribution of ψ_α is

$$|\psi_\alpha|^2 = |b_0|^2 + 2|b_0 b_2| \cos\phi_{02} P_2(\cos\theta') + |b_2|^2 [P_2(\cos\theta')]^2 . \qquad (18)$$

The phase difference ϕ_{02} is very near zero or π; the deviation being small, it may be taken as 0 or π according to Tolhoek.[44] The relative phase of b_0 and b_2 is the same as the relative phase of a_0 and a_2, the probability amplitudes at great distance. Thus, if the S and D waves are in phase the intensity is maximum at the poles of the spheroid.

Since the amplitudes of the different partial waves enter into the angular distributions, experiments on oriented nuclei would be of significance in testing the different theoretical predictions regarding these amplitudes. Thus, by taking into account effects due to the quadrupole moment and coriolis forces,[46,47] a 25% enhancement of the D-wave admixture has been predicted for U^{233} over that predicted by the approximate Bohr-Froman-Mottelson relation.[48] A similar enhancement is expected for E^{253}.

Theoretical predictions involve specific nuclear models employed for the alpha-decay process. More complete theoretical discussions of the decay process, including the effect of angular momentum, have been given by Rasmussen and Segall,[49] Froman,[50] Steenberg and Sharma,[45] Brussard and Tolhoek,[44] and Pennington and Preston.[51]

C. Theoretical Angular Distribution of Alpha Particles from E^{253}

The relevant decay scheme for E^{253} is given in Fig. 15a. The "favored" transition is the only one considered. This represents 97.2% of the alpha particles from E^{253}. It is assumed that the remaining 3% gives an isotropic distribution. The partial-wave intensities calculated by Asaro are given in Table II.[52] If we assume that only one magnet substate, $I_z = \pm 7/2$, is populated at the lowest temperature studied (this will be justified later), the total angular distribution is given by

(a) L = 0, 2 in phase, L = 2, 4 out of phase

$$W(\theta) = 1 + 0.921\ P_2(\cos\theta) - 0.010\ P_4(\cos\theta)$$

(b) L = 0, 2 in phase, L = 2, 4 in phase

$$W(\theta) = 1 + 1.061\ P_2(\cos\theta) + 0.103\ P_4(\cos\theta)$$

(c) L = 0, 2 out of phase, L = 2, 4 in phase

$$W(\theta) = 1 - 0.663\ P_2(\cos\theta) + 0.013\ P_4(\cos\theta)$$

(d) L = 0, 2 out of phase, L = 2, 4 out of phase

$$W(\theta) = 1 - 0.803\ P_2(\cos\theta) + 0.080\ P_4(\cos\theta)$$

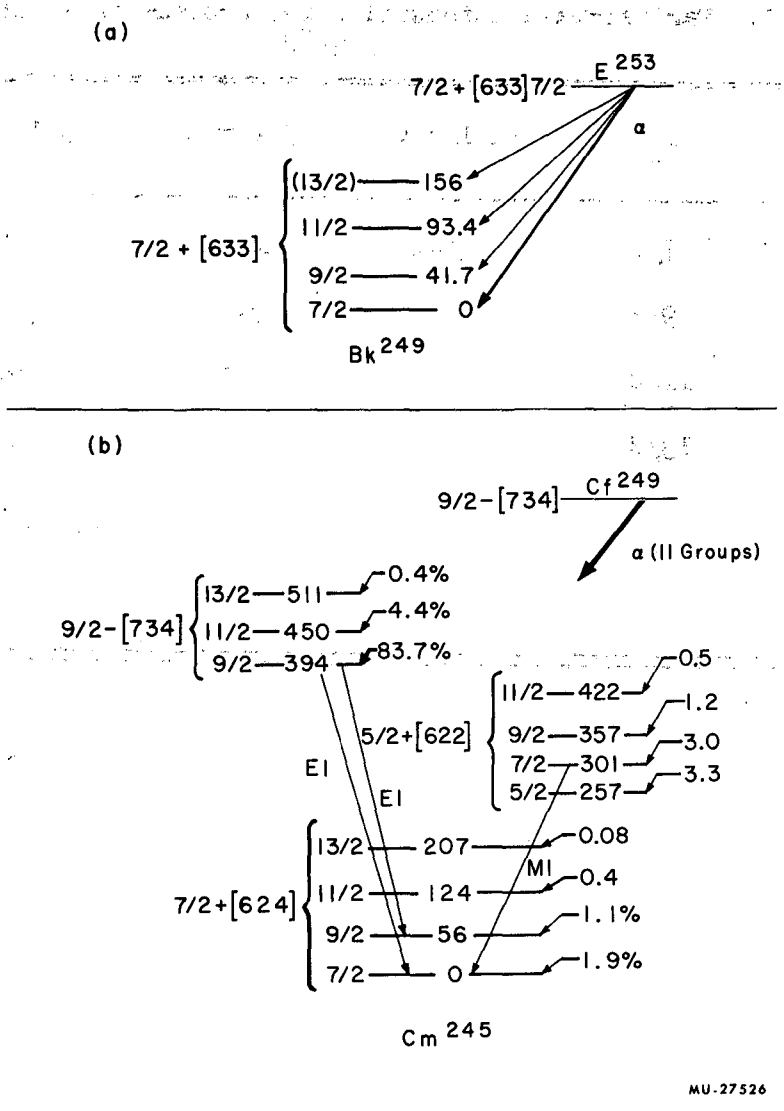

Fig. 15. (a) Partial decay scheme of E^{253}; (b) decay scheme of Cf^{249}.

Table II. Partial-wave intensities for ground-state alpha transitions in E^{253}

I_i	I_f	% L = 0	% L = 2	% L = 4	Total
7/2	7/2	79.6	10.0	0.1	89.7
7/2	9/2		5.9	0.3	6.2
7/2	11/2		0.9	0.3	1.2
7/2	13/2			0.11	0.11
				Total	97.21

D. Theoretical Angular Distribution of Alpha Particles from Californium-249

The relevant decay scheme is given in Fig. 15b. The "favored" transition group to the 9/2 - band is composed of 80% L = 0 and 20% L = 2 waves, with hindrance factors of 4.5 and 14, respectively. The group to the 5/2 + band has a composition of 87% L = 3 and 13% L = 5 waves, with hindrance factors of 150 and 350, respectively. The alpha waves going to the ground state (7/2 +) band is a mixture of 25% L = 1, 67% L = 3 and 8% L = 5. The hindrance factors are 3.1×10^4, 6.9×10^3, and 2.2×10^4 for the L = 1, 3, and 5 waves, respectively.[53] From the above data, the partial-wave intensities to the various rotational levels were calculated by using the method of Bohr, Froman, and Mottelson.[48] These are given in Table III. The theoretical distribution, assuming $I_z = \pm 9/2$ lies lowest, is given in Table IV with the corresponding choices of phases.

Table III. Partial-wave intensities of alpha groups from Cf^{249}

(a) Favored transition to the 9/2 - band

I_i	I_f	% L = 0	% L = 2	Total
9/2	9/2	70.8	12.9	83.7
9/2	11/2		4.4	4.4
9/2	13/2		0.4	0.4
			Total	88.5

(b) Transition to the 5/2 + rotational band

I_i	I_f	% L = 3	% L = 5	Total
9/2	5/2	3.2	0.1	3.3
9/2	7/2	2.65	0.35	3.0
9/2	9/2	0.84	0.36	1.2
9/2	11/2	0.22	0.28	0.5
			Total	8.0

(c) Transition to the 7/2 + (ground state) rotational band

I_i	I_f	% L = 1	% L = 3	% L = 5	Total
9/2	7/2	0.77	1.1	0.04	1.91
9/2	9/2	0.09	0.91	0.10	1.1
9/2	11/2	0.005	0.294	0.101	0.4
9/2	13/2		0.038	0.042	0.08
				Total	3.49

Table IV. Theoretical Angular distribution of alpha particles from oriented Cf^{249}

$W(\theta)$ $x = \cos\theta$	Relative phase				
	L = 0, 2 9/2 - band	3, 5 5/+ + band	1,3 7/2 + band	3,5	1,5
$1 + 1.114\ P_2(x) + 0.29\ P_4(x)$	in	in	in	in	in
$1 + 1.176\ P_2(x) + 0.26\ P_4(x)$	in	in	out	out	in
$1 + 1.147\ P_2(x) + 0.27\ P_4(x)$	in	in	out	in	out
$1 + 1.143\ P_2(x) + 0.30\ P_4(x)$	in	in	in	out	in
$1 + 1.197\ P_2(x) + 0.28\ P_4(x)$	in	out	in	in	in
$1 + 1.259\ P_2(x) + 0.25\ P_4(x)$	in	out	out	out	in
$1 + 1.230\ P_2(x) + 0.26\ P_4(x)$	in	out	out	in	out
$1 + 1.226\ P_2(x) + 0.29\ P_4(x)$	in	out	in	out	out

VIII. EXPERIMENTAL RESULTS

A. Einsteinium-253

The experimental data for einsteinium are compiled in Table V, with geometry corrections where available[54] (see footnotes in Table V). Figure 16a shows the plot of $[W(\theta) - 1]$ as a function of $1/T$ for the complete data after normalizing the saturation value of each run to the average value obtained with the collimated samples. The values used were:

$$[W(\theta) - 1] = + 0.70$$

for the 0 deg distribution and

$$[W(\theta) - 1] = - 0.31_5$$

for the 90 deg distribution.

The solid curves are for the above values of the distribution for a spin Hamiltonian of the form $\mathcal{H} = AS_zI_z$, for $|A'/k| = 0.40^{\circ}K$. The broken curves are for a spin Hamiltonian of the form $\mathcal{H} = B(S_xI_x + S_yI_y)$ for $|B'/k| = 0.40^{\circ}K$. Figure 16 b, c, and d shows plots of $[W(\theta) - 1]$ as a function of $1/T$ for the uncollimated runs. The solid lines in each case is the best fit for the spin Hamiltonian $\mathcal{H} = AS_zI_z$ for a spin of $I_z = \pm 7/2$. For each run, a value of $|A'/k|$ was obtained giving the average value of

$$|A'/k| = 0.40 \pm 0.04^{\circ}K.$$

Table V. Angular distribution of alpha particles from oriented E^{253}

Date	No.	1/T	W(θ)		W(θ) - 1	
			0 deg	90 deg	0 deg	90 deg
7-30-61[a]	1	33.7	1.574		0.574	
	2	35.7	1.599		0.599	
	3	19.5	1.548		0.548	
	4	14.5	1.590		0.590	
	5	8.7	1.469		0.469	
	6	7.3	1.431		0.431	
	7	5.7	1.394		0.394	
	8	3.7	1.293		0.293	
	9	9.2	1.477		0.477	
	10	11.5	1.525		0.525	
11-10-61[b]	1	30	1.727		0.727	
	2	13.8	1.709	0.676	0.709	-0.324
	3	11.2	1.625	0.670	0.625	-0.330
	4	3.7	1.304	0.801	0.304	-0.199
	5	8.7	1.584	0.683	0.584	-0.317
	6	8.5	1.596	0.668	0.596	-0.332
	7	10.2	1.662	0.710	0.662	-0.290
	8	12.5	1.658	0.672	0.658	-0.328
12-15-62[b]	1	39	1.544	0.686	0.544	-0.314
	2	19	1.532	0.694	0.532	-0.306
	3	9	1.443	0.738	0.443	-0.262
	4	38.5	1.560	0.679	0.560	-0.321
	5	9.7	1.368	0.801	0.368	-0.199
	6	25	1.513	0.685	0.513	-0.315
	7	10.2	1.480	0.724	0.480	-0.276
	8	6.5	1.437	0.778	0.437	-0.222
	9	37.5	1.566	0.681	0.566	-0.319

Table V. (cont'd)

Date	No.	1/T	W(θ)		W(θ) - 1	
			0 deg	90 deg	0 deg	90 deg
12-20-61[a]	1	12.4		0.716		-0.284
	2	20.1		0.706		-0.294
	3	16.5		0.735		-0.265
	4	18.2		0.760		-0.240
	5	9.4		0.729		-0.271
	6	7.2		0.752		-0.248
	7	4.3		0.802		-0.198
	8	5.7		0.868		-0.132
	9	8.2		0.755		-0.245
	10	5		0.861		-0.139
	11	1.5		0.905		-0.095
	12	1.9		0.912		-0.088
	13	6.7		0.808		-0.192
	14	12.2		0.727		-0.273
	15	17.5		0.703		-0.297
	16	9.5		0.735		-0.265
	17	39.2		0.662		-0.338
1-10-62[c]	1	38.8	1.665	0.704	0.665	-0.296
	2	31.9	1.709	0.716	0.709	-0.284
	3	33.2	1.678	0.699	0.678	-0.301
	4	33.5	1.739	0.668	0.739	-0.332
	5	36	1.733	0.696	0.733	-0.304
	6	33.2	1.718		0.718	
	7	33.8	1.699	0.640	0.699	-0.360
Average[d]					0.70	-0.31_5

[a]Uncollimated source, no solid-angle correction made

[b]Uncollimated source, solid-angle correction made

[c]Collimated source, solid angle correction made

[d]Average of collimated-source data

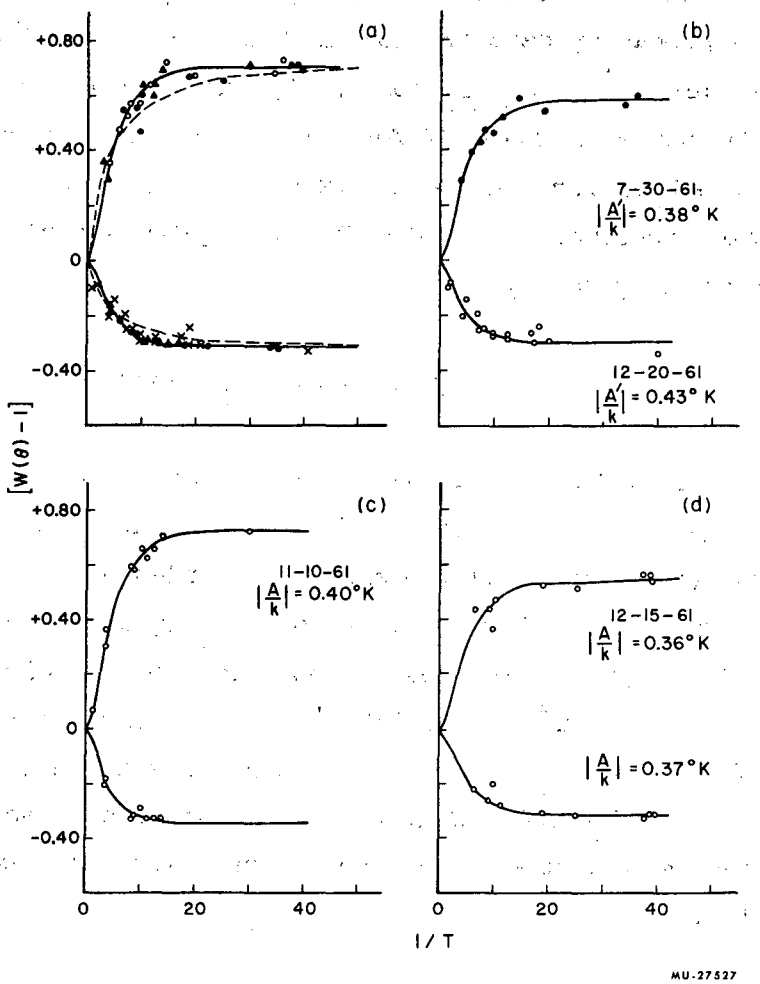

Fig. 16. (a) Consolidated data of alpha-particle distribution from aligned E^{253} fitted to the saturation value obtained from the collimated sample vs 1/T; (b,c,d) alpha-particle intensity distributions from aligned E^{253} vs 1/T.

B. Californium-249

Figure 17 shows a typical gamma-ray spectrum from Cf^{249}. The 394-keV gamma-ray data are compiled in Table VI. Figure 18a, b, and c shows plots of $B_2G_2U_2F_2$ for the 394-keV γ-ray as a function of 1/T (see footnotes in Table VI for description of each run). Figure 18d shows $B_2G_2U_2F_2$ for the 394-keV gamma ray taken during the alpha-particle experiments. At 0.02°K the angular distribution of the 394-keV γ-ray is given by

$$W(\theta) = 1 + (0.14_6 \pm 0.04)\ P_2\ (\cos\theta).$$

The 340-keV γ-ray has an anisotropy of opposite sign to that of the 394-keV γ-ray. Because of its low intensity, it was not possible to get a very good temperature dependence.

Table VII lists the data for the alpha-particle distribution from Cf^{249}. Figure 19a and b shows plots of the alpha particle distribution as a function of 1/T for the two experimental runs. In each case the solid curve corresponds to an asymptotic value of the coefficient of $P_2(\cos\theta)$ of 1.52, with an adjustable value for $|A'/k|$. From the temperature dependence of the anisotropy, we get a value for $|A'/k|$ of

$$\left|\frac{A'}{k}\right| = 0.035 \pm 0.004\ ^\circ K.$$

At 0.03°K, the alpha-particle anisotropy may be approximated by

$$W(\theta) = 1 + (0.64 \pm 0.08)\ P_2\ (\cos\theta).$$

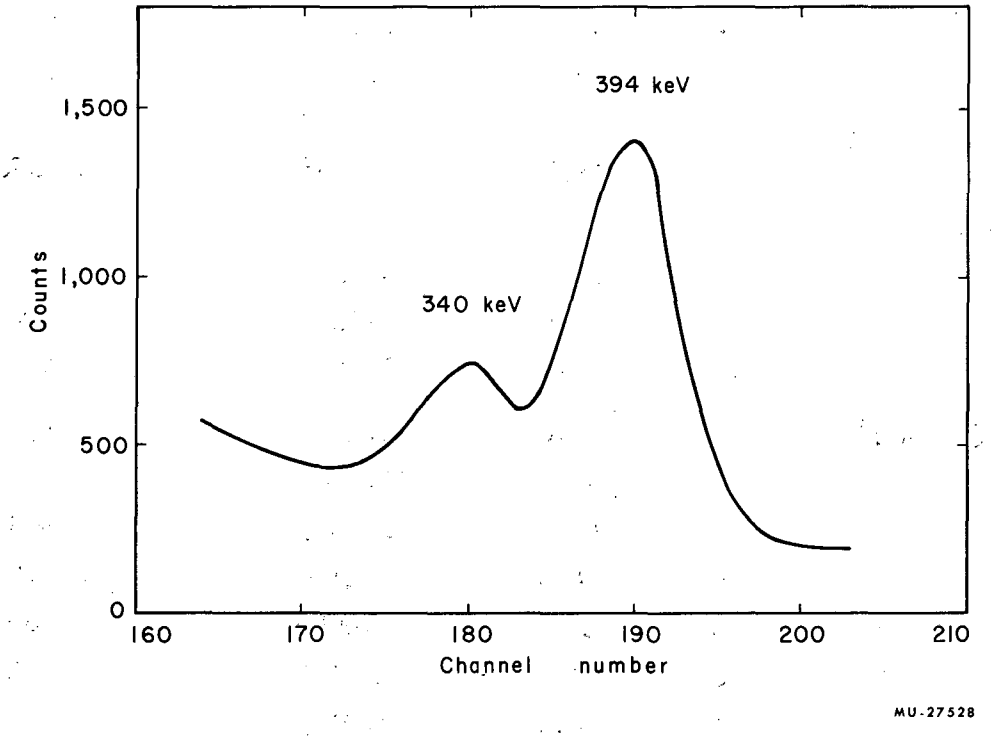

Fig. 17. Typical gamma-ray spectrum of Cm^{245}.

Table VI. Anisotropy of the 394-keV gamma ray

Date	No.	1/T	W(θ = 0 deg)	$G_2B_2U_2F_2$ (θ = 0 deg)
8-11-60[a]	1	52.5	1.1279	0.1279
	2	53.5	1.1565	0.1565
	3	57	1.1569	0.1569
	4	44.5	1.1116	0.1116
	5	30.4	1.0946	0.0946
	6	22.7	1.0839	0.0839
	7	15.6	1.0068	0.0068
	8	54.2	1.1415	0.1415
	9	57	1.1500	0.1500
	10	55.8	1.1367	0.1367
	11	55.8	1.1450	0.1450
8-12-60[a]	1	53.6	1.1703	0.1703
	2	46	1.1443	0.1443
	3	41	1.0655	0.0655
	4	34.4	1.1146	0.1146
	5	28.7	1.0680	0.0680
	6	21	1.0120	0.0120
	7	14.7	1.0183	0.0183
	8	18.1	1.0252	0.0252
	9	22.5	1.0514	0.0514
	10	34.5	1.1335	0.1335
	11	40.5	1.1033	0.1033
9-8-60[a]	1	54.5	1.1323	0.1323
	2	44.5	1.1234	0.1234
	3	39.7	1.1214	0.1214
	4	32.7	1.0868	0.0868
	5	44.5	1.1221	0.1221
	6	26.5	1.0745	0.0745
	7	18.2	1.0465	0.0465
	8	40.5	1.1093	0.1093
	9	32.7	1.0782	0.0782
	10	53.6	1.1249	0.1249

Table VI (cont'd).

Date	No.	1/T	W(θ = 0 deg)	$G_2B_2U_2F_2$ (θ = 0 deg)
9-4-60[a]	1	56	1.1826	0.1826
	2	45.3	1.1407	0.1407
	3	39.5	1.1430	0.1430
	4	32	1.0513	0.0513
	5	57	1.1328	0.1328
4-11-62[b]	1	22.7	1.090	0.090
	2	28	1.051	0.051
	3	28.8	1.030	0.030
	4	21.9	1.050	0.050
	5	17	1.018	0.018
	6	10.6	1.013	0.013
	7	16.7	1.061	0.061
	8	20.7	1.086	0.086
	9	26.3	1.101	0.101
	10	30.3	1.116	0.116
	11	15.3	1.067	0.067
	12	14	1.029	0.029
	13	7.6	1.012	0.012
5-15-62[c]	1	44.2	1.077	0.077
	2	42.6	1.086	0.086
	3	17.6	1.052	0.052
	4	31.5	1.049	0.049
	5	23	1.074	0.074
	6	29.6	1.085	0.085

Table VI (cont'd).

Date	No.	1/T	W(θ = 0 deg)	$G_2B_2U_2F_2$ (θ = 0 deg)
5-17-62[c]	1	38.2	1.099	0.099
	2	26.6	1.078	0.078
	3	32.5	1.096	0.096
	4	22.2	1.065	0.065
	5	15.8	1.037	0.037
	6	20.6	1.041	0.041

[a] Volume-distributed source

[b] Activity deposited as thin film on single spot on crystal for alpha experiment

[c] Inactive coating of neodymium ethylsulfate grown outside crystal used used for alpha experiment

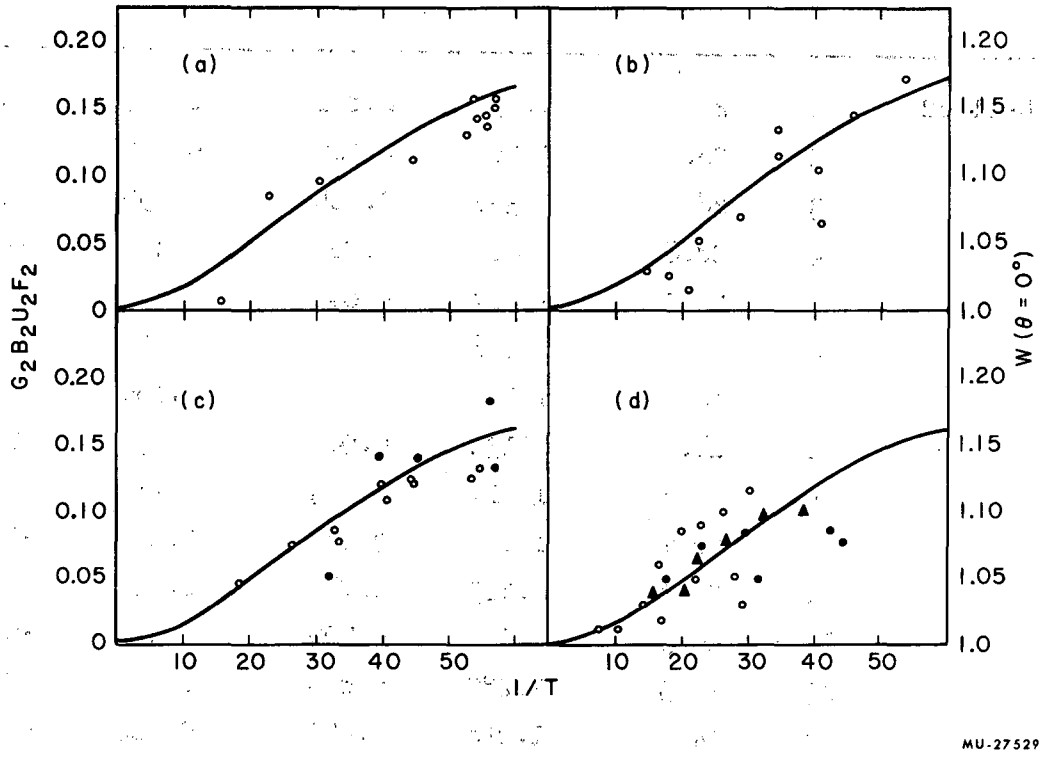

Fig. 18. Plot of $G_2B_2U_2F_2$ of the 394-keV γ ray of Cm^{245} as a function of 1/T. (a,b,c) from volume-distributed sources; (d) taken during the alpha-particle runs.

Table VII. Alpha-particle angular distribution from oriented Cf^{249}

Date	No.	1/T	W(θ)		W(θ) - 1	
			0 deg	90 deg	0 deg	90 deg
4-11-62	1	22.7	1.257	0.811	0.257	-0.189
	2	26.6	1.389	0.766	0.389	-0.234
	3	28	1.356	0.784	0.356	-0.216
	4	28.8	1.426	0.760	0.426	-0.240
	5	21.9	1.407	0.844	0.407	-0.156
	6	17	1.176		0.176	
	7	10.6	1.156		0.156	
	8	14.8	1.132	0.966	0.132	-0.034
	9	16.7	1.214	0.883	0.214	-0.117
	10	20.7	1.299	0.878	0.299	-0.259
	11	26.3	1.419	0.741	0.419	-0.259
	12	30.3	1.507	0.700	0.507	-0.300
	13	15.3	1.287	0.864	0.287	-0.136
	14	14	1.226	0.875	0.226	-0.125
	15	12.4	1.258	0.927	0.258	-0.073
	16	7.6	1.132		0.132	
	17	7	1.130		0.130	
	18	32.5	1.585	0.658	0.585	-0.342
4-16-62	1	25.6	1.452	0.772	0.452	-0.228
	2	28.2	1.586	0.721	0.586	-0.279
	3	29	1.567	0.747	0.567	-0.253
	4	19.3	1.326	0.871	0.326	-0.129
	5	18.2	1.280		0.280	
	6	23.5	1.496	0.789	0.496	-0.211
	7	15.9	1.308	0.850	0.308	-0.150
	8	19.4	1.542	0.816	0.542	-0.184

Table VII (cont'd).

Date	No.	1/T	W(θ)		W(θ) - 1	
			0 deg	90 deg	0 deg	90 deg
	9	13.3	1.314	0.874	0.314	-0.126
	10	11	1.264	0.930	0.264	-0.070
	11	14	1.165		0.165	
	12	10	1.372	0.898	0.372	-0.102
	13	31.3	1.732	0.698	0.732	-0.302
	14	25.1	1.473	0.761	0.473	-0.239
	15	26.9	1.454	0.730	0.454	-0.270
	16	24.3	1.465	0.760	0.465	-0.240
	17	20.6	1.355	0.790	0.355	-0.210
	18	24.3	1.412	0.803	0.412	-0.197

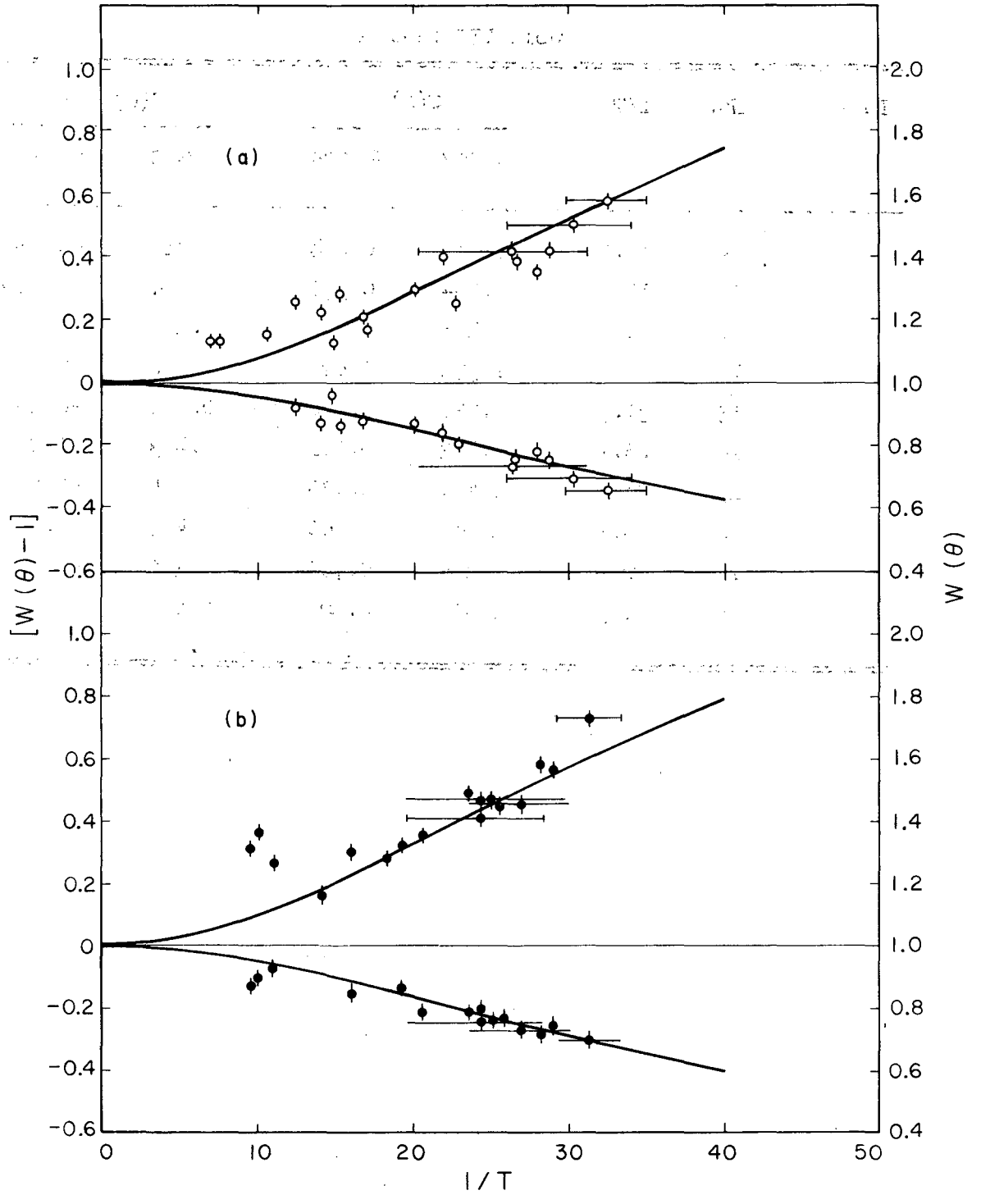

Fig. 19. Alpha-particle distribution from aligned Cf^{249} vs 1/T. (a) April 11, 1962; (b) April 16, 1962.

IX. DISCUSSION

A. Nuclear Alignment of Einsteinium

1. Electronic ground state of einsteinium

Because einsteinium is chemically analogous to holmium, E^{3+} may be expected to have the same electronic ground state as Ho^{3+}, which has the configuration $4f^{10}$ and the ground level $^4I_8$. Baker and Bleaney have studied paramagnetic resonance with Ho^{165} in an yttrium ethylsulfate lattice, for which they give the following Hamiltonian[55]

$$\mathcal{H} = g_{\parallel}\mu_B H_z S_z + g_{\perp}\mu_B (H_x S_x + H_y S_y) + A S_z I_z + B(S_x I_x + S_y I_y)$$

$$+ \Delta_x S_x + \Delta_y S_y + P\left[I_z^2 - \frac{1}{3} I_0 (I_0 + 1)\right], \qquad (20)$$

with $g_{\parallel} = 15.36$; $g_{\perp} \approx 0$; $A/k = 0.478 \pm 0.002^{\circ}K$; $B/k = 0.03^{\circ}K$; $P/k = 0.001^{\circ}K$; $\Delta/k = (\Delta_x^2 + \Delta_y^2)^{1/2}/k = 0.09 \pm 0.02^{\circ}K$.

By extrapolation of the crystal field parameters and using the theory of Elliott and Stevens, they suggested that two states lie lowest (a) the doublet which is principally $|\pm 7\rangle$ with small admixtures of $|\pm 1\rangle$ and $|\mp 5\rangle$ and (b) a singlet characterized by the mixture of the $|\pm 6\rangle$ and $|0\rangle$ states.

It can easily be shown that in zero field, the dominating term in the Hamiltonian for Ho^{3+} in the ethylsulfate lattice is AS_zI_z, for which axial alignment would result, that is, $I_z = \pm I_0$ would lie lowest. Although the terms in B, P, and Δ are nonvanishing, their contributions may be neglected because they are sufficiently small compared to A. Postma et al. aligned Ho^{166m} in a neodymium ethylsulfate lattice and found that below $0.05^{\circ}K$ the γ-anisotropies are independent of temperature.[56] At $0.025^{\circ}K$, they assumed that the nuclei were completely aligned. They also showed that the contribution from the B term would amount to multiplication of the effect by a factor very close to unity.

To find out if the spin Hamiltonian for Ho^{3+} can be applied to E^{3+}, we need a theoretical prediction of the ground state for the latter. We assumed that E^{3+} has the configuration $5f^{10}$ and the ground level $^4I_8$. The crystal field parameters for E^{3+} in the ethylsulfate lattice were obtained in the following manner. From the crystal field parameters of several rare-earth ions in the ethylsulfate lattice,[57-59] an extrapolation was made to get the crystal field parameters for Ho^{3+} in this lattice. The crystal field parameters for tripositive holmium were multiplied by the ratios of the parameters for americium trichloride to those of europium ethylsulfate, which represent the change from 5f to 4f shells. The change from chloride to the ethylsulfate lattice was corrected for by multiplying by the ratios of the parameters for $Pr(C_2H_5SO_4)_3 \cdot 9H_2O$ to $PrCl_3$.[60]

After multiplication of the holmium-crystal field parameters by these two sets of ratios, we obtain some estimate of the crystal field parameters for tripositive einsteinium in the ethylsulfate lattice. The values obtained by this method, which were used in the estimation of the ground state for E^{3+}, are:

$$A_2^0 \langle r^2 \rangle = +348 \text{ cm}^{-1}$$

$$A_4^0 \langle r^4 \rangle = -71 \text{ cm}^{-1}$$

$$A_6^0 \langle r^6 \rangle = -86 \text{ cm}^{-1}$$

$$A_6^6 \langle r^6 \rangle = +1650 \text{ cm}^{-1}.$$

The eigenfunctions and eigenvalues resulting from the crystal-field splitting of the ground term are tabulated in Table VIII and plotted in Fig. 20.

Table VIII. Eigenstates and eigenvalues for the ground term of E^{3+} in neodymium ethylsulfate, resulting from crystal-field splitting.

Wave function, $\|^4I_8 , J_z\rangle$	Energy (cm^{-1})	Degeneracy
$0.54 \|\pm 6\rangle + 0.65\|0\rangle$	-459	1
$0.78 \|\pm 7\rangle + 0.54\|\pm 1\rangle + 0.32\|\mp 5\rangle$	-431	2
$0.15 \|\pm 8\rangle + 0.77\|\pm 2\rangle + 0.62\|\mp 4\rangle$	-223	2
$-0.61 \|\pm 7\rangle + 0.53\|\pm 1\rangle + 0.59 \mp 5\rangle$	-205	2
$0.71 \|+ 6\rangle - 0.71\|- 6\rangle$	-187	1
$0.71 \|\pm 3\rangle$	-180	1
$-0.98 \|\pm 8\rangle + 0.04\|\pm 2\rangle + 0.20\|\mp 5\rangle$	+122	2
$-0.46 \|\pm 6\rangle + 0.63\|\ 0\rangle$	+178	1
$-0.14 \|\pm 7\rangle + 0.65\|\pm 1\rangle - 0.75\|\mp 5\rangle$	+316	2
$0.12 \|\pm 8\rangle + 0.64\|\pm 2\rangle - 0.76\|\mp 5\rangle$	+478	2
$0.71 \|+ 3\rangle - 0.71\|- 3\rangle$	+530	1

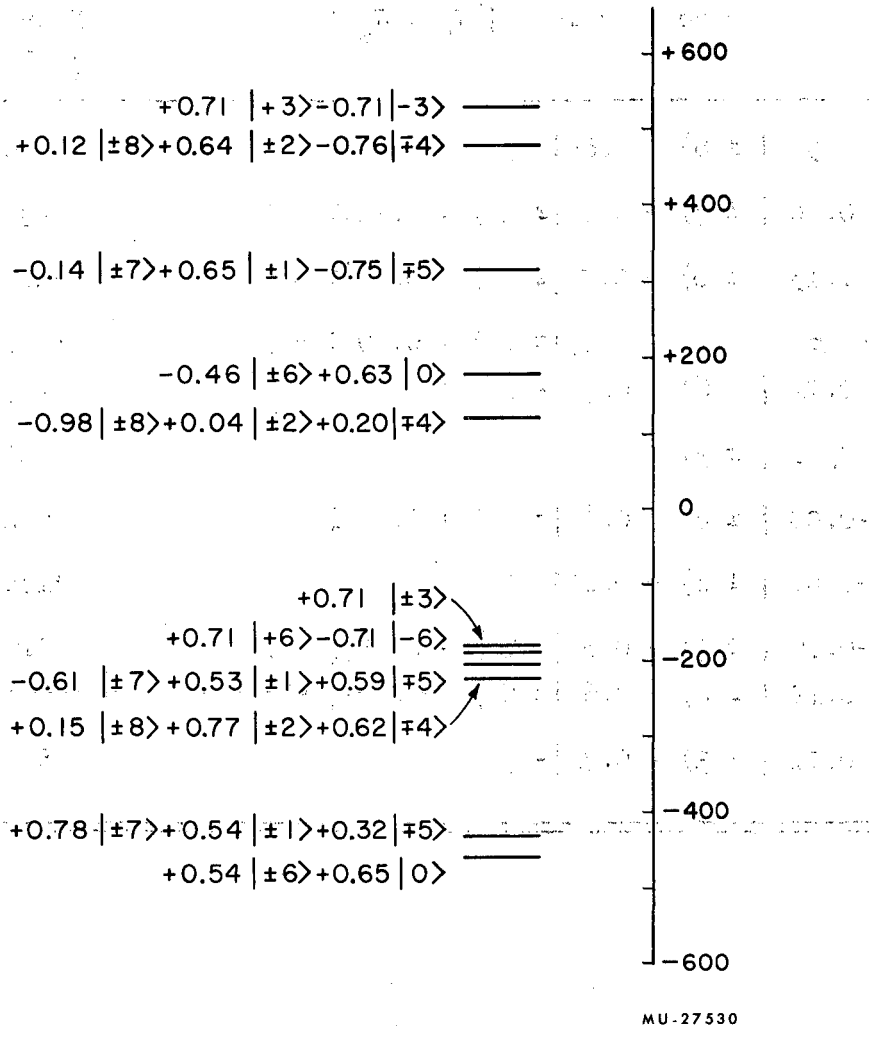

Fig. 20. Electronic energy levels and wavefunctions for tripositive einsteinium in a neodymium ethylsulfate lattice.

From this calculation, either of two states could lie lowest. The higher states are about 200 cm^{-1} away and can be omitted in the discussion of the ground state. The two states that could equally well be the ground state are (a) the doublet, which in the $|J_z\rangle$ notation is approximated by $0.78\,|\pm 7\rangle + 0.54\,|\pm 1\rangle + 0.32\,|\mp 5\rangle$, and (b) a singlet approximated by $0.54\,|\pm 6\rangle + 0.65\,|0\rangle$. Since there are no states for which $\Delta J_z = \pm 1$, we have $g_\perp = 0$ for both of these states, the doublet (a) has $g_\parallel = 10.1$, while the singlet (b) would of course have $g_\parallel = 0$. No alignment would result if the singlet were the ground state. This leaves the doublet (a) as the ground state for E^{3+}.

Since E^{3+} and Ho^{3+} were found to have essentially the same electronic ground state, the spin Hamiltonian for the latter may be used as the spin Hamiltonian of E^{3+}. The dominant term in the spin Hamiltonian of Ho^{3+} is

$$\mathcal{H} = AS_zI_z \,. \qquad (11)$$

There may be other terms in the E^{3+} spin Hamiltonian, just as in holmium, but these are likely to be small. A term which may be non-vanishing and significant, but still small compared to the A term, is that due to the Jahn-Teller splitting. This effect would split the ground doublet, and permit admixture of the single level with one of the states of the doublet. This effect is responsible for the lifting of the (accidental) degeneracy in non-Kramers ions.

The alpha-particle distribution from einsteinium was found to be highly anisotropic and is saturated at fairly high temperatures. Essentially complete alignment is indicated at $0.05^{\circ}K$. The magnitude and temperature dependence of the alpha-particle distribution implies a nuclear orientation mechanism very similar to that of Ho^{165}. Even the derived value of $|A'|/k$ is nearly the same as that for Ho^{165}. It should be noted that the temperature dependence of the intensity distribution is axial rather than planar (see Fig. 16a). This is also borne out by the vanishing theoretical value of $g_\perp$.

The Hamiltonian expressed by Eq. (11), which was found to be a good approximation of the spin Hamiltonian for E^{3+}, would lead to axial alignment. In einsteinium, this would indicate that the substate $I_z = 7/2$ would lie lowest, and the hyperfine structure constant A/k can be evaluated by using the matrix elements of the electronic-ground-state doublet, and the theory of Elliott and Stevens. The theoretical value of the hfs constant is given by

$$A/k = 4.20 \times 10^{-27} \langle r^{-3} \rangle (\mu/I_0)\ ^{\circ}K, \qquad (21)$$

where $\langle r^{-3} \rangle$ is the expectation value for the 5f electrons, I_0 is the nuclear spin, and μ is the nuclear magnetic moment. The direction of preferential emission can be determined as follows. In this region of the periodic table, where nuclei are strongly prolately deformed, there is abundant experimental and theoretical evidence that the nuclear symmetry axis for intrinsic nuclear states such as the ground states of Cf^{249} and E^{253}. Since we have axial alignment, the angular-momentum vector is directed along the crystalline c-axis. We observed that enhanced alpha-particle emission also occurred in this direction. The experimental results thus establish unambiguously that the alpha particles are emitted preferentially along the nuclear symmetry axis, which for a prolate spheroid is in the direction of the polar regions. This agrees with the prediction of Hill and Wheeler and also with the results obtained by Dabbs et al. for Np^{237}.

Since we get preferential emission in the direction of the polar regions, the S and D waves must be in phase. The relative phase of the L = 2, 4 waves may be inferred also from the angular distribution. The experimental data give $[W(0^{\circ}) - 1]/[1 - W(90^{\circ})] = 2.1$. Theoretically, for this ratio we get (a) 1.96 for the L = 2, 4 waves out of phase and (b) 2.37 for the L = 2, 4 in phase. The experimental result is much nearer to the former, that is, the L = 2, 4 waves are out of phase in E^{253}.

B. Nuclear Alignment of Californium

1. The Attenuation Factor

When a nucleus emits a particle during radioactive decay a certain amount of recoil energy is imparted to the daughter nucleus. In beta decay, the disintegration energy is carried mostly by the beta particle and neutrino, and the daughter nucleus gets very little recoil energy. However, in alpha-particle decay, the recoil may be substantial. In the alpha decay of Cf^{249}, the Cm^{245} daughter has about 95 keV of recoil energy. This corresponds to a velocity of 20 cm per μsec for the recoil. The recoil is also estimated to have a range of about 50 unit cells of the neodymium ethylsulfate lattice. If the 394-keV gamma ray has a lifetime $\tau = 10^{-14}$ sec., the recoil could traverse about 5 unit cells before the gamma ray is emitted. Therefore, during the lifetime of the 394-keV state, the recoil nucleus could be subjected to various interactions such as collisions with the ions in the vacuum space, collisions with the ions in the ethylsulfate lattice, and various magnetic and electric interactions inside and outside of the crystal lattice. These effects would tend to reorient the spin of the daughter nucleus, leading to a reduced observed anisotropy for the emitted gamma ray.

In the study of alpha-gamma correlation in Am^{241}, Am^{243}, and Cm^{243}, Flamm found that the correlation was highly attenuated.[61] In Am^{243}, for example, she found that there was a marked attenuation of correlation for nuclei recoiling into vacuun, and almost no anisotropy for nuclei recoiling into Mylar. The attenuation coefficients below the "hard-core" value for a static interaction which were obtained in vacuum indicated that fluctuating magnetic or electric field gradients were present at the daughter nucleus during the recoil motion.

2. Gamma-Ray Anisotropies in Cf^{249} and the Spin Hamiltonian

In the previous section it was shown that alpha-gamma correlation is considerably attenuated when the intermediate state has a finite lifetime. Perturbations which would tend to reorient the spin of the recoiling nucleus would also be expected in Cf^{249}, just as was found in

the alpha decay of Am^{241}, Am^{243}, and Cm^{243}. We must then include an attenuation coefficient G_k in the expression for the angular distribution of gamma rays from aligned Cf^{249}.

The angular distribution of the gamma rays, which is preceded by the emission of alpha particles from aligned nuclei, could then be expressed by

$$W(\theta) = \sum_{\text{even}} G_k B_k U_k F_k P_k (\cos\theta). \qquad (22)$$

For low degrees of alignment, terms in $k > 2$ may often be neglected.

The decay scheme and spin assignments for the levels in Cf^{249} decay is fairly well-established (cf. Fig. 15b). The 394-keV γ-ray has the spin sequence 9/2 - (L = 0, 2) 9/2 - (E1) 7/2 +. For this spin sequence, we have $U_2F_2 = +0.2247$ and the γ-ray angular distribution is given by

$$W(\theta) = 1 + 0.2247\ G_2B_2P_2(\cos\theta). \qquad (23)$$

This may also be written as

$$W(\theta) = 1 + X_2P_2(\cos\theta)\ , \qquad (23a)$$

where X_2 is the experimentally observed coefficient of $P_2(\cos\theta)$. The orientation parameter B_2 is a function of a single parameter $\beta = A/2kT$. From the temperature dependence of the alpha-particle anisotropy, one can obtain the hfs constant A/k, which can then be used to determine the value of B_2 at any particular temperature. Since we know B_2, we can obtain the attenuation coefficient G_2, by comparing Eq. (23) to (23a). For the coefficient G_2, we obtained a value of 0.64 to which we should attach an error of about 15%, which arises from uncertainties in the value of $|A'|/k$ and the experimentally observed gamma anisotropy.

For the 340-keV γ-ray, the spin sequence is given by 9/2 - (L = 0, 2) 9/2 - (E1) 9/2 +. For this spin sequence, $U_2F_2 = -0.331$ and the angular distribution of this gamma ray is then given by

$$W(\theta) = 1 - 0.331\, G_2B_2P_2(\cos\theta). \qquad (24)$$

Since the two gamma rays are emitted from the same intermediate state, U_2 and B_2 would be the same for them. The attenuation coefficient may also be expected to have an equal value.

To determine the appropriate spin Hamiltonian representing the interaction responsible for nuclear alignment in Cf^{3+}, we could use the analogy between E^{3+} and Ho^{3+}. We have shown that the spin Hamiltonian for Ho^{3+} is a very good approximation to that of E^{3+}. In a similar manner, we may infer that the spin Hamiltonian for Cf^{3+}, could be approximated by the spin Hamiltonian for Dy^{3+}. For the latter,[62] it has been shown that the dominant term of the Hamiltonian in the neodymium ethylsulfate lattice is given by Eq. (11), viz. $\mathcal{H} = AS_zI_z$. The electronic ground state for Cf^{3+} would also be expected to be expected to be very similar to that of Dy^{3+}. To confirm the assumption that these two ions have similar forms of the spin Hamiltonian, we look at the gamma-ray anisotropy. For axial alignment, the temperature-dependent term B_2 is positive. From Eqs. (23) and (24), we see that the 394-keV γ-ray should show positive anisotropy, while the 340-keV γ-ray should have the opposite sign. It was found that this is indeed the case. The sign and temperature-dependence of the γ-ray anisotropy is very similar to that of Dy^{3+}. From this similarity and the analogy between E^{3+} and Ho^{3+}, we can infer that Cf^{3+} has essentially the same electronic ground state as Dy^{3+}, and therefore analogous forms for the spin Hamiltonian. However, it would not be possible to determine the other terms in the Hamiltonian, which again may be expected to be very small. The spin Hamiltonian expressed by Eq. (11) would lead to axial alignment, with the state $I_z = \pm 9/2$ lying lowest. From the ground-state expression (cf. p. 41) and the theory of Elliott and Stevens, we

can estimate the hfs constant A/k. For this we get

$$A/k = 4.35 \times 10^{-27} \langle r^{-3} \rangle (\mu/I_0)^{\circ}K , \qquad (25)$$

where again $\langle r^{-3} \rangle$ is the expectation value for the 5f electrons, and μ is the nuclear magnetic moment.

3. Alpha-Particle Angular Distribution from Aligned Cf^{249}

Just as in E^{253}, the alpha-particle was highly anisotropic, although not saturated at the lowest temperature attained in the experiments. It was shown in the preceding discussion of the γ-ray anisotropy that nuclear alignment of Cf^{249} is axial, which would lead to the alignment of the nuclear angular-momentum vector along the crystalline c-axis. The observed enhancement of alpha emission in this direction is another confirmation that the alpha particles are emitted along the direction of the angular-momentum vector. For prolately deformed nuclei, the nuclear angular-momentum vector is in the same direction as the nuclear-symmetry axis, that is, in the direction of the "tips" of the spheroid. As in the einsteinium isotope, preferential emission from the polar regions is indicated--another independent confirmation of the prediction of Hill and Wheeler.

Since preferential emission occurred at the poles of the spheroid, the S and D waves are in phase. The contribution from the other branches are sufficiently small that it would not affect this conclusion. It was not possible to determine with any certainty the relative phases of the odd-angular-momentum components of the partial waves to the other branches, although an out-of-phase relationship is indicated in the L = 3, 5 components to the 5/2 + band.

C. Magnetic Moments of E^{253} and Cf^{249}

To determine the magnetic moments from the experimental data, one needs a reasonable estimate of $\langle r^{-3} \rangle$ for the 5f electrons. This parameter was calculated by Foglio and Pryce[63] for elements 91 through 96 for net ionic charges of n~1 and n~5. The parameter for the tripositive species was determined by assuming a linear dependence of $\langle r^{-3} \rangle$ on the net ionic charge. The values obtained by interpolation were extrapolated to get the values for E^{3+} and Cf^{3+}.

The magnetic moment of E^{253} arises mostly from the odd proton. The nuclear spin of this isotope is $I_0 = 7/2$. From Eq. (21) and the experimentally determined value of $|A'|/k$, we obtain

$$|\mu|_{E^{253}} = 4.9 \text{ n.m.},$$

with

$$\langle r^{-3} \rangle = 68 \text{Å}^{-3}.$$

The nuclear spin of Cf^{249} is $I_0 = 9/2$ and due to an odd neutron. From Eq. (25) and the experimentally determined value of $|A'|/k$, we get

$$|\mu|_{Cf^{249}} = 1.3 \text{ n.m.},$$

with

$$\langle r^{-3} \rangle = 58 \text{Å}^{-3}$$

Errors of about 20%, of which one-half comes from uncertainties in the theory, should be attached to these values.

It is interesting to compare these experimentally determined moments with theory. The Nilsson states for E^{253} and Cf^{249} are $7/2 + [633]$ and $9/2 - [734]$, respectively. Using the value 0.33

for the gyromagnetic ratio, g_R, for both isotopes, and the deformation parameters $\delta = 0.24$ and 0.23 for E^{253} and Cf^{249}, respectively, we obtain

$$(\mu)_{E^{253}} \text{ (theory)} = + 4.2 \text{ n.m.}$$

$$(\mu)_{Cf^{249}} \text{ (theory)} = - 0.89 \text{ n.m.}$$

ACKNOWLEDGMENTS

I wish to thank:

Prof. David A. Shirley, who directed this research and introduced me to the techniques of nuclear orientation. His suggestions, comments, aid, and patience in discussing the many problems encountered were indispensable in carrying out and interpreting these experiments.

Prof. John O. Rasmussen, who suggested this field of research and directed its early phase. His comments and interest in this work were a great help.

My wife, for her inspiration and encouragement.

Messrs. William L. Hansen and Leo Schifferle, whose aid in the preparation of the alpha counters was responsible for the successful termination of this work.

Mr. Edward Woo, whose experience in applied electronics was often called upon during the whole course of this research.

I am indebted to:

Drs. B. B. Cunningham and J. C. Wallman for the loan of the californium sample.

Dr. S. G. Thompson and Messrs. L. Philipps, R. Gatti, and R. Brandt for providing the carrier-free einsteinium samples.

I am grateful to my colleagues and their families for their hospitality and friendship.

Finally, I wish to express my thanks to the numerous personnels of the Chemistry Department and the Laboratory, and the many American families, who made the visit to this country, a most pleasant experience for myself and my family.

This work was done under the auspices of the U. S. Atomic Energy Commission.

REFERENCES

1. James F. Schooley, Some Low-Temperature Nuclear Orientation Studies, UCRL-9296, July 1960.
2. James N. Haag, Nuclear Alignment Experiments on Cerium Radioisotopes, UCRL-9872, September 1961.
3. Carolyn A. Lovejoy, Nuclear Orientation of Some Rare-Earth Isotopes, UCRL-9747, June 1961.
4. F. S. Goulding and W. L. Hansen, Leakage Current in Semiconductor Junction Radiation Detectors and Its Influence on Energy-Resolution Characteristics UCRL-9436, November 1960.
5. F. J. Walter, J. W. T. Dabbs, and L. D. Roberts, Rev. Sci. Instr. 31, 756 (1960).
6. F. J. Walter, J. W. T. Dabbs, L. D. Roberts, and H. W. Wright, A Study of Germanium Surface Barrier Counters, O. R. N. L. CF-58-11-99, November 1958.
7. Earl K. Hyde, The Radioactive Decay of the Isotopes of the Transuranium Elements, UCRL-9148, January 1961.
8. E. K. Hyde and G. T. Seaborg, "The Transuranium Elements," in Handbuch der Physik, S. Flugge, Ed. (Springer-Verlag, Berlin, 1957), Vol. 42, p. 274.
9. Horst Meyer, Phil. Mag. 2, 521 (1957).
10. Carolyn A. Lovejoy, private communication.
11. K. W. H. Stevens, Proc. Phys. Soc. (London) A65, 209 (1952).
12. R. J Elliott and K. W. H. Stevens, Proc. Roy. Soc. (London) A215, 437 (1952).
13. R. J. Elliott and K. W. H. Stevens, Proc. Roy. Soc. (London) A218, 553 (1953).
14. R. J. Elliott and K. W. H. Stevens, Proc. Roy. Soc. (London) A219, 387 (1953).
15. B. R. Judd and I. P. K. Lindgren, Phys. Rev. 122, 1802 (1961).
16. T. P. Gray and G. R. Satchler, Proc. Phys. Soc. (London) A68 349 (1955).

17. M. Ferentz and N. Rosenzweig, Table of F Coefficients, ANL-5324, 1955.

18. R. J. Blin-Stoyle and M. A. Grace, "Oriented Nuclei," in Handbuch der Physik, S. Flugge, Ed. (Springer-Verlag, Berlin, 1957), p. 556.

19. K. S. Toth and J. O. Rasmussen, Phys. Rev. 115, 150 (1959).

20. K. S. Toth and O. B. Nielsen, private communication.

21. J. W. Mihelich, B. Harmatz, and T. H. Handley, Phys. Rev. 108, 989 (1957).

22. See reference 14 and M. J. D. Powell and R. Orbach, Proc. Phys. Soc. (London) A78, 752 (1961).

23. J. M. Baker and B. Bleaney, Proc. Phys. Soc. (London) A245, 156 (1958).

24. J. G. Park, cited in reference 25.

25. A. H. Cooke, D. T. Edmonds, F. R. McKim, and W. P. Wolf, Proc. Roy. Soc. (London) A252, 246 (1959).

26. B. R. Mottelson and S. G. Nilsson, Kgl. Danske Videnskab. Selskab, Mat.-fys. Medd. 1, 8 (1959).

27. S. G. Nilsson and O. Prior, Kgl. Danske Videnskab. Selskab., Mat.-fys. Medd. 32, No. 16 (1961).

28. B. R. Mottelson and S. G. Nilsson, Kgl. Danske Videnskab. Selskab, Mat.-fys. Skrifter 1, No. 8 (1959).

29. David R. Speck, Phys. Rev. 101, 1725 (1956).

30. W. Low, Phys. Rev. 103, 1309 (1956).

31. J. O. Rasmussen and L. W. Chiao, in Proceedings of the International Conference on Nuclear Structure, Kingston, Canada, 1960, D. A. Bromley and E. W. Vogt, Eds. (University of Toronto Press, Toronto, Canada, 1960), Chap. 6, pp. 646-649.

32. J. A. Spiers, Nature 161, 807 (1948).

33. D. L. Hill and J. A. Wheeler, Phys. Rev. 89, 1133 (1953).

34. L. D. Roberts, J. W. T. Dabbs, G. W. Parker, and R. D. Ellison, Bull. Am. Phys. Soc. 1, 207 (1956).

35. J. W. T. Dabbs, L. D. Roberts, and G. W. Parker, Physica 24, S69 (1958).

36. L. D. Roberts, J. W. T. Dabbs, and G. W. Parker, in Proceedings of the Second United Nations International Conference on the Peaceful Uses of Atomic Energy, Geneva, 1958 (United Nations, Geneva, 1958), Vol. 15, p. 322.

37. S. H. Hanauer, J. W. T. Dabbs, L. D. Roberts, and G. W. Parker, Phys. Rev. 124, 1512 (1961).

38. P. M. Llewellyn, cited in reference 37.

39. B. Bleaney, P. M. Llewellyn, M. H. L. Pryce, and G. R. Hall, Phil. Mag. 45, 992 (1954).

40. J. C. Eisenstein and M. H. L. Pryce, Proc. Roy. Soc. (London) A229, 20 (1955).

41. M. H. L. Pryce, Phys. Rev. Letters 3, 375 (1959).

42. L. D. Roberts and J. W. T. Dabbs, Bull. Am. Phys. Soc. 5, 22 (1960).

43. M. E. Rose, Elementary Theory of Angular Momentum, (John Wiley and Sons, Inc., New York, 1957) p. 176.

44. P. J. Brussard and H. A. Tolhoek, Physica 24, 233 (1958).

45. N. R. Steenberg and R. C. Sharma, Can. J. Phys. 38, 290 (1960).

46. R. R. Chasman and J. O. Rasmussen, Phys. Rev. 115, 1257 (1959).

47. J. O. Rasmussen, Bull. Am. Phys. Soc. II, 6, 232 (1961).

48. A. Bohr, P. O. Froman, and B. R. Mottelson, Danske Videnskab. Selskab, Mat.-fys. Medd. 29, No. 10 (1955).

49. J. O. Rasmussen and B. Segall, Phys. Rev. 103, 1298 (1956).

50. P. O. Froman, Kgl. Danske Videnskab. Selskab, Mat.-fys. Skrifter 1, No. 3 (1957).

51. E. M. Pennington and M. A. Preston, Can. J. Phys. 36, 944 (1958).

52. F. Asaro, S. G. Thompson, F. S. Stephens, and I. Perlman, cited in reference 7.

53. F. Asaro, F. S. Stephens, and I. Perlman, cited in reference 7.

54. M. E. Rose, Geometrical Corrections for Anisotropically Emitting Sources, ORNL-2050, March 1956.

55. J. M. Baker and B. Bleaney, Proc. Phys. Soc. (London) A68, 1090 (1955).

56. H. Postma, A. R. Miedema, and M. C. Eversdijk Smulders, Physica 25, 671 (1959).

57. Brian R. Judd, Mol. Phys. 2, 407 (1959).

58. M. J. D. Powell and R. Orbach, Proc. Phys. Soc. (London) A78, 753 (1961).

59. J. M. Baker and B. Bleaney, Proc. Roy. Soc. (London) A245, 156 (1958).

60. Brian R. Judd, Proc. Roy. Soc. (London) A241, 414 (1957).

61. Eileen Flamm, Perturbation of Alpha- Gamma Corrections in Transuranium Isotopes, UCRL-9325, August 1960.

62. Q. O. Navarro and D. A. Shirley, Phys. Rev. 123, 186 (1961).

63. M. E. Foglio and M. H. L. Pryce, Mol. Phys. 4, 287 (1961).